ORIGINAL ARTICLE

VIPP2 interacts with VIPP1 and HSP22E/F at chloroplast membranes and modulates a retrograde signal for *HSP22E/F* gene expression

Jasmine Theis[1] | Justus Niemeyer[1] | Stefan Schmollinger[1] | Fabian Ries[2] |
Mark Rütgers[1] | Tilak Kumar Gupta[3] | Frederik Sommer[1] |
Ligia Segatto Muranaka[1] | Benedikt Venn[1] | Miriam Schulz-Raffelt[1] |
Felix Willmund[2] ⓘ | Benjamin D. Engel[3][†] ⓘ | Michael Schroda[1] ⓘ

[1]Molekulare Biotechnologie & Systembiologie, TU Kaiserslautern, Kaiserslautern, Germany

[2]Molecular Genetics of Eukaryotes, TU Kaiserslautern, Kaiserslautern, Germany

[3]Department of Molecular Structural Biology, Max Planck Institute of Biochemistry, Martinsried, Germany

Correspondence
Michael Schroda, Molekulare Biotechnologie & Systembiologie, TU Kaiserslautern, Paul-Ehrlich Straße 23, D-67663 Kaiserslautern, Germany.
Email: schroda@bio.uni-kl.de

[†]Present address: Helmholtz Pioneer Campus, Helmholtz Zentrum München, 85764 Neuherberg, Germany

Funding information
Deutsche Forschungsgemeinschaft, Grant/Award Numbers: SFB/TRR175, FOR2092

Abstract

VIPP proteins aid thylakoid biogenesis and membrane maintenance in cyanobacteria, algae, and plants. Some members of the Chlorophyceae contain two VIPP paralogs termed VIPP1 and VIPP2, which originate from an early gene duplication event during the evolution of green algae. VIPP2 is barely expressed under nonstress conditions but accumulates in cells exposed to high light intensities or H_2O_2, during recovery from heat stress, and in mutants with defective integration (*alb3.1*) or translocation (*secA*) of thylakoid membrane proteins. Recombinant VIPP2 forms rod-like structures in vitro and shows a strong affinity for phosphatidylinositol phosphate. Under stress conditions, >70% of VIPP2 is present in membrane fractions and localizes to chloroplast membranes. A *vipp2* knock-out mutant displays no growth phenotypes and no defects in the biogenesis or repair of photosystem II. However, after exposure to high light intensities, the *vipp2* mutant accumulates less HSP22E/F and more LHCSR3 protein and transcript. This suggests that VIPP2 modulates a retrograde signal for the expression of nuclear genes *HSP22E*/F and *LHCSR3*. Immunoprecipitation of VIPP2 from solubilized cells and membrane-enriched fractions revealed major interactions with VIPP1 and minor interactions with HSP22E/F. Our data support a distinct role of VIPP2 in sensing and coping with chloroplast membrane stress.

KEYWORDS
high light response, membrane stress, molecular chaperones, protein homeostasis, reactive oxygen species, retrograde signalling, thylakoid membrane biogenesis

1 | INTRODUCTION

VIPP1 is a highly conserved protein found in cyanobacteria and chloroplasts. In cyanobacteria, VIPP1 localizes to the cytoplasm, the

plasma membrane, and the thylakoid membranes (Fuhrmann, Bultema, et al., 2009; Srivastava, Pisareva, & Norling, 2005). In chloroplasts, VIPP1 localizes to the stroma, the chloroplast envelope, and the thylakoid membranes (Kroll et al., 2001; Li, Kaneko, & Keegstra, 1994; Liu et al., 2005; Zhang, Kato, Otters, Vothknecht, & Sakamoto, 2012). VIPP1 evolved from the bacterial phage shock protein PspA, with which it shares several structural features. Both proteins consist of α-helical domains connected by random-coil spacers, but VIPP1 possess an additional domain of about 30 amino acids at its C-terminus (Otters et al., 2013; Westphal, Heins, Soll, & Vothknecht, 2001). In both PspA and VIPP1, the N-terminal 24 amino acids form an amphipathic α-helix (AHa) that is required for membrane binding and the formation of larger oligomers (Gao, Wang, Zhang, & Liu, 2015; Jovanovic et al., 2014; McDonald, Jovanovic, Ces, & Buck, 2015; McDonald, Jovanovic, Wallace, Ces, & Buck, 2017; Otters et al., 2013). In vitro, both proteins form higher order oligomers of >1 MDa that give rise to rings and rods (Aseeva et al., 2004; Fuhrmann, Bultema, et al., 2009; Hankamer, Elderkin, Buck, & Nield, 2004; Liu et al., 2007; Male, Oyston, & Tavassoli, 2014; Saur et al., 2017). Rods formed by recombinant VIPP1 from _Chlamydomonas_ can engulf liposomes containing physiological amounts of phosphatidylinositol phosphate (Theis, Gupta, et al., 2019). PspA and VIPP1 may also assemble into higher order oligomers in vivo, as both proteins form cellular puncta that can be seen by fluorescence microscopy (Engl et al., 2009). In cyanobacteria, VIPP1 punctae dynamically form at or near highly curved thylakoid membranes during discrete events of oligomerization and de-oligomerization between the cytosolic and membrane-bound forms of VIPP1, with high light (HL) intensities shifting the equilibrium towards the latter (Bryan et al., 2014; Gutu, Chang, & O'Shea, 2018). In chloroplasts, VIPP1 localizes close to envelope and thylakoid membranes in a variety of patterns, including dots, lines, forks, crosses, five-point stars, and webs (Aseeva et al., 2004; Li et al., 1994; Nordhues et al., 2012; Zhang et al., 2012; Zhang, Kondo, Kamikubo, Kataoka, & Sakamoto, 2016). At the chloroplast envelope, these structures are dynamically assembled and disassembled under osmotic stress (Zhang et al., 2012; Zhang, Kondo, et al., 2016).

In the absence of membrane stress, PspA has been shown to negatively control its own expression by binding to the transcriptional activator PspF via its amphipathic α-helix b (AHb, residues 25–42; Jovanovic et al., 2014). When PspA detects lipid packing stress in membranes by its AHa, it releases PspF and forms higher-order oligomers that serve as the effector complex. Via AHa, PspA oligomers bind to membranes suffering lipid packing stress and prevent proton leakage (Jovanovic et al., 2014; Kleerebezem, Crielaard, & Tommassen, 1996; Kobayashi, Suzuki, & Yoshida, 2007; McDonald et al., 2015; McDonald et al., 2017).

The function of VIPP1 appears to be more complex, as mutant plants, algae, and cyanobacteria that express less or no VIPP1 display highly pleiotropic phenotypes. VIPP1 was originally proposed to be involved in the biogenesis of the lipid part of thylakoid membranes by playing a role in membrane vesicle traffic, which led to its naming as Vesicle-Inducing Protein in Plastids (Aseeva et al., 2007; Kroll et al., 2001; Westphal et al., 2001). This view has been questioned, and

VIPP1 is now widely believed to function in coping with chloroplast membrane stress (Zhang et al., 2012; Zhang, Kondo, et al., 2016; Zhang, Kusaba, Tanaka, & Sakamoto, 2016) as well as in the biogenesis and repair of thylakoid membrane protein complexes (Fuhrmann, Gathmann, Rupprecht, Golecki, & Schneider, 2009; Gao & Xu, 2009; Gutu et al., 2018; Lo & Theg, 2012; Nordhues et al., 2012; Walter, Hristou, Nowaczyk, & Schunemann, 2015; Zhang & Sakamoto, 2013; Zhang, Shen, Li, Golbeck, & Bryant, 2014). It was recently proposed that the AHa of PspA evolved specifically for the binding to stressed membranes and VIPP1's affinity for anionic lipids (Hennig et al., 2015) might be the key to its role in the biogenesis and repair of thylakoid membrane complexes (McDonald et al., 2017).

Members of the Chlorophyceae encode a paralog of VIPP1, termed VIPP2, with both proteins sharing only 55% identical residues. Many land plants, including _Arabidopsis thaliana_, encode only a single VIPP1 protein. The question addressed in this study is why some members of the Chlorophyceae have evolved and maintained two VIPP paralogs.

2 | MATERIALS AND METHODS

2.1 | Phylogenetic analyses

VIPP/PspA protein sequences were identified by sequence comparison using protein blast (BLASTP 2.3.0+, BLOSUM62, E-threshold −1) and obtained from Phytozome 12 (https://phytozome.jgi.doe.gov), CyanoBase (http://genome.microbedb.jp/cyanobase/), the National Center for Biotechnology Information, EnsemblProtists (http://protists.ensembl.org), EnsemblPlants (http://plants.ensembl.org), the Cyanophora Genome Project (http://cyanophora.rutgers.edu), the Klebsormidium Genome Project (http://www.plantmorphogenesis.bio.titech.ac.jp/), and from the Online Resource for Community Annotation of Eukaryotes (OrcAE, http://bioinformatics.psb.ugent.be/orcae/overview/Ectsi). Gene models were manually evaluated and start and termination sites were adjusted for _Galdieria sulphuraria_ and _Ostreococcus lucimarinus_, respectively. Sequences were preliminarily aligned using CLUSTALW (http://www.genome.jp/tools-bin/clustalw) to identify the chloroplast targeting sequences of the eukaryotic proteins and to trim the less-conserved N-terminal transit sequences. The alignment was imported into GeneDoc. The trimmed sequences and sequence IDs can be found in Table S1. The sequences were then aligned with ClustalWS (Gonnet matrix, gapext = 0.1, endgaps = 0.5, gapdist = 1, gapopen = 10, transition weighting = 0.5) in Jalview (www.jalview.org; Waterhouse, Procter, Martin, Clamp, & Barton, 2009) and the alignment imported into MEGA7 (Kumar, Stecher, & Tamura, 2016). The evolutionary history was inferred using the Neighbor-Joining method (Saitou & Nei, 1987) using 1,000 replicates for the bootstrap test (Felsenstein, 1985). The evolutionary distances were computed using the Poisson correction method (Zuckerkandl & Pauling, 1965) and are in the units of the number of amino acid substitutions per site. All positions with less than 95% site coverage were eliminated. That is, fewer than 5% alignment gaps, missing data, and

ambiguous bases were allowed at any position. There were a total of 211 positions in the final dataset.

2.2 | Cloning

The VIPP2 coding region lacking the chloroplast transit peptide was amplified by polymerase chain reaction (PCR) from cDNA clone BP094145 (Asamizu et al., 2000) using primers 5′-ggactagtgctc ttcgaaCGCCAATCTGTTTGCCCGGGTTGCGC-3′ and 5′-caccctcgaGT CCCTTCACTCCCGCGCCCGGC-3′ (mismatches in lowercase letters). The 850-bp PCR product was digested with SapI and XhoI and cloned into SapI–XhoI-digested pTYB11 (New England Biolabs), giving pMS510. Four fragments of the genomic VIPP2 gene (Cre11. g468050) ranging from start to stop codon were amplified by PCR on genomic DNA from wild-type strain CC-4533 using primers 5′-ttgaagacATaATGCATTTGGCAGGTGATTC-3′ and 5′-ttgaagacGT CcTCCTGCATCTCCTCCGCCAC-3′ for 879-bp fragment 1, 5′-ttga agacAGGAgGACATGATGCGAATGCGCCA-3′ and 5′-ttgaagacAAGAt GGAGGATGTGCGTGGGGAA-3′ for 202-bp fragment 2, 5′-ttgaagac TCCaTCTTCCCTGTCCACCTCCTT-3′ and 5′-ttgaagaCCAGCGACGTC TTGGCACTGGC-3′ for 1,552-bp fragment 3, and 5′-ttgaagacCGTCG CTGGCGCTGCAGGAGA-3′ and 5′-ttgaagacTCCgaaCcCTCCCGaG CCCGGCGCCGGAGCTCC-3′ for 1,352-bp fragment 4. All four PCR products were combined with destination vector pAGM1287 (Weber, Engler, Gruetzner, Werner, & Marillonnet, 2011), digested with BbsI, and directionally assembled by ligation into level 0 construct pMBS277. The latter was then combined with plasmids pCM0-022 (VIPP2 promoter +5′UTR), pCM0-100 (3xHA), pCM0-119 (RPL23 3′UTR) from the Chlamydomonas Modular Cloning (MoClo) kit (Crozet et al., 2018) as well as with destination vector pICH47742 (Weber et al., 2011), digested with BsaI and ligated to generate level 1 construct pMBS360 harbouring the full VIPP2 transcription unit. For the NanoLUC reporter constructs, plasmids pCM0-013 (βTUB2 promoter +5′UTR) and pCM0-041 (βTUB2 first intron), or pCM0-022 (VIPP2 promoter +5′UTR) were combined with plasmids pCM0-061 (NanoLUC), pCM0-100 (3xHA), pCM0-119 (RPL23 3′UTR), and destination vector pICH47742, digested with BsaI and ligated to generate level 1 constructs pMBS409 (βTUB2::NanoLUC) and pMBS281 (VIPP2::NanoLUC). All three level 1 constructs were then combined with pCM1-01 (level 1 construct with the aadA gene conferring resistance to spectinomycin flanked by the PSAD promoter and terminator) from the Chlamydomonas MoClo kit, with plasmid pICH41744 containing the proper end-linker, and with destination vector pAGM4673 (Weber et al., 2011), digested with BbsI, and ligated to yield level 2 constructs pMBS361 (aadA + VIPP2 gene), pMBS410 (aadA + βTUB2::NanoLUC), and pMBS289 (aadA + VIPP2::NanoLUC). Correct cloning was verified by Sanger sequencing.

2.3 | Expression and purification of recombinant VIPP1 and VIPP2

VIPP1 (pMS319) was expressed as a C-terminal fusion to a chitin-binding domain/intein in ER2566 cells after inducing expression with 5-mM IPTG for 6 hr at 30°C and purified under native conditions according to the manufacturer's instructions (New England Biolabs) with an additional washing step with 5-mM Mg-ATP. For the purification of VIPP2, ER2566 cells containing pMS510 were pelleted after induction and resuspended in lysis buffer (50-mM Tris–HCl, pH 8.0, 100-mM NaCl, 5-mM EDTA, 0.5% (v/v) Triton X-100, 0.25× protease inhibitor [Roche]). The cell suspension was sonicated for 2 min on ice, and 2-mM $MgSO_4$ was added to chelate EDTA. The solution was supplemented with 0.01-mg ml^{-1} DNAse I and 0.1-mg ml^{-1} lysozyme and incubated at 25°C for 20 min. Inclusion bodies were collected by centrifugation (15 min at 19,000g). The resuspension, sonication, and centrifugation procedures were repeated four times using lysis buffer with 0.5% (v/v) Triton X-100 followed by two additional washes in lysis buffer lacking Triton X-100. Finally, the inclusion bodies were dissolved in 6-M Urea, 20-mM Tris pH 8. Eluted VIPP1 and VIPP2 proteins were concentrated in Amicon Ultra-15 centrifugal filter devices (Millipore) followed by dialysis with 200-mM NaCl, 75-mM NaSCN, and 20-mM Tris–HCl, pH 7.5 overnight, then with 50-mM NaCl, 75-mM NaSCN, 20-mM Tris–HCl, pH 7.5 for another 4 hr according to Hankamer et al. (2004). Proteins were frozen in liquid nitrogen and stored at −80°C.

2.4 | Electron microscopy

Samples containing 0.2–0.7 mg ml^{-1} heterologously expressed VIPP1 or VIPP2 were negatively stained with 2% (w/v) uranyl acetate. Examination of specimens was performed with a 200-kV Tecnai F20 transmission electron microscope (FEI) equipped with a 4K Eagle CCD camera (FEI). The electron micrographs were recorded at 50,000× nominal magnification (object pixel size of 2.21 Å), with around 5-μm defocus. Images were binned once to a pixel size of 4.42 Å

2.5 | Strains and cultivation conditions

Chlamydomonas reinhardtii strain CC-4533 (cw15, mt–), the vipp2 mutant strain derived from CC-4533 (LMJ.RY0402.174411), CC-124, and CC-3054 (ac29, alb3.1) were obtained from the Chlamydomonas Resource Center (https://www.chlamycollection.org/). Strains CF185 and cw15-325 were described in Schroda, Vallon, Wollman, and Beck (1999) and Schmollinger, Strenkert, and Schroda (2010), respectively. Cultures were maintained mixotrophically in Tris-acetate-phosphate (TAP) medium (Kropat et al., 2011) on a rotatory shaker at 25°C and ~30 μmol photons m^{-2} s^{-1}. CF185 and the vipp2 mutant were transformed via the glass bead method (Kindle, 1990) with level 2 plasmids and plated onto TAP agar plates containing 100-μg ml^{-1} spectinomycin. High-light treatments were done with 150-ml cultures grown to mid-logarithmic phase placed in 400-ml beakers on a rotary shaker and illuminated with ~1,000 μmol photons m^{-2} s^{-1} by Osram HLX 250-W 64663 Xenophot bulbs. A glass plate, nonpermissive to infrared and UV irradiation, was placed between light sources and beakers and cooled by ventilation. Beaker positions were swapped at regular

intervals during the experiment to ensure equal illumination. A water-cooled metal plate beneath the beakers allowed maintaining a temperature of 25°C in the cultures. For heat stress, cells were pelleted by centrifugation at 25°C and 1,300g for 2 min, resuspended in prewarmed TAP medium, and incubated in a water bath under agitation and constant illumination. Light intensities were determined using a Luxmeter (Heinz Walz).

2.6 | Protein analyses

For whole-cell protein extraction, cells were pelleted and resuspended in 75-mM Tris–HCl pH 6.8, 2% (w/v) SDS, 10% (v/v) glycerol, boiled for 1 min at 96°C, and centrifuged. After protein quantification according to Lowry, Rosebrough, Farr, and Randall (1951), Laemmli buffer (Laemmli, 1970) was added and proteins subjected to SDS-PAGE and semidry blotting onto nitrocellulose-membranes. Immunodetection was performed by enhanced chemiluminescence (ECL) using the FUSION-FX7 Advance™ imaging system (PeqLab). Antisera were against VIPP1 (Liu et al., 2005), VIPP2 (this study), HSP70B and CGE1 (Schroda, Vallon, Whitelegge, Beck, & Wollman, 2001), CF1β (Lemaire & Wollman, 1989), LHCA2 (Agrisera AS01 006), PsbA (Agrisera AS05 084), SECA (Schroda M., unpublished), HSP22F (Rütgers et al., 2017), DEG1C (Theis, Lang, et al., 2019), HA (Abcam ab137838), PsaA (Agrisera AS06 172), cytochrome f (Pierre & Popot, 1993), HSP90C (Willmund & Schroda, 2005), and LHCSR3 (Naumann et al., 2007). Anti-rabbit-HRP (Sigma-Aldrich) was used as secondary antibody. Protein-lipid overlay assays were performed as described previously (Theis, Gupta, et al., 2019).

2.7 | Immunofluorescence microscopy

For immunofluorescence microscopy, cells were fixed and stained as described previously (Uniacke, Colon-Ramos, & Zerges, 2011) with minor modifications: Microscopy slides were washed twice for 10 min with 100% ethanol. To enhance adherence of the cells to the slides, slides were coated with 0.1% poly-L-lysine. Cells were fixed with 4% formaldehyde for at least 2 hr at 25°C on an overhead rotator. Aliquots of 40-μl cell suspension were allowed to adhere to the microscope slides for 7 min at 25°C, followed by incubation in 100% methanol for 6 min at −20°C. Afterwards, slides were washed three times with phosphate-buffered saline (PBS) for 5 min each. Cell permeabilization was achieved by incubating the slides with 2% Triton X-100 in PBS for 10 min at 25°C. Slides were washed three times with PBS containing 5-mM MgCl$_2$ and with PBS–BSA (PBS, 1% BSA) for at least 30 min at 25°C. Slides were incubated over night at 4°C with antisera against HA, HSP70B in 1:100 and 1:5000 dilutions in PBS–BSA, respectively. Slides were then washed twice with PBS for 10 min at 25°C followed by incubation in a 1:200 dilution of the tetramethylrhodamine-isothiocyanate-labelled goat anti-rabbit antibody (Sigma- Aldrich) in PBS–BSA for 2 hr at 25°C. Finally, the slides were washed three times with PBS for 5 min each, and a mounting solution containing DAPI (Vectashield) was dispersed over the cells. Images were captured with an Olympus BX53 microscope with filters for DAPI and tetramethylrhodamine-isothiocyanate and an Olympus DP26 colour camera.

2.8 | RNA extraction and qRT-PCR

RNA was isolated from about 5×10^7 cells with the NucleoSpin® RNA Plant kit (Macherey-Nagel) using the manufacturer's protocol. The quality of the RNA preparations was estimated by agarose gel electrophoresis, and RNA concentration and purity were determined spectrophotometrically (NanoDrop-1,000). cDNA synthesis was performed using the M-MLV reverse transcriptase (Promega), deoxynucleotide triphosphate, and oligo-d(T)18 primers. Real-time reverse transcription-PCR (qRT-PCR) was performed using the StepOnePlus RT-PCR system (Applied Biosystems) and the 5× HOT FIREPol® EvaGreen® qPCR Supermix kit from Solis BioDyne. Each reaction contained the vendor's master mix, 200 nM of each primer, and cDNA corresponding to 10-ng input RNA in the reverse transcriptase reaction. Primers used for CBLP2 and HSP22F amplicons are described in Strenkert, Schmollinger, Sommer, Schulz-Raffelt, and Schroda (2011), those for the LHCSR3.1 amplicon in Maruyama, Tokutsu, and Minagawa (2014). The reaction conditions were as follows: 95°C for 10 min, followed by cycles of 95°C for 15 s, 65°C for 20 s, and 72°C for 20 s, up to a total of 40 cycles.

2.9 | Cell fractionation

Approximately 2×10^7 cells were harvested by centrifugation and resuspended in TE buffer (10 mM Tris–HCl pH 8.0, 1-mM EDTA) supplemented with 0.25× protease inhibitor (Roche). An aliquot was taken for whole-cell proteins, whereas the remainder was subjected to 3–4 cycles of freezing in liquid nitrogen and thawing at 25°C. Disrupted cells were centrifuged for 30 min at 18,000g and 4°C. The supernatant was collected as soluble protein fraction. Pellets were resuspended by sonication with the same volume of TE buffer containing either 1% (w/v) α-dodecyl maltoside (α-DDM; Adipogen) or 2% (v/v) Triton X-100. After centrifugation for 30 min at 18,000g and 4°C, the supernatant was taken as solubilized membrane protein fraction. Pellets were resuspended by sonication with the same volume of TE buffer and taken as fraction with nonsolubilized material.

2.10 | Immunoprecipitations

Chlamydomonas wild-type and *vipp2-c* cells were *grown to midlogarithmic phase* and either exposed to 800 μmol photons m^{-2} s^{-1} for 5 hr or supplemented with 2-mM H$_2$O$_2$ for 4 hr. Cells were harvested by centrifugation at 1,000g and 4°C. Cells treated with HL were resuspended in lysis buffer (20-mM Hepes-KOH, pH 7.2, 10-mM KCl, 1-mM MgCl$_2$, 154-mM NaCl, 0.25× protease inhibitor cocktail

[Roche]) and broken by sonication. Intact cells and cell debris were removed by centrifugation for 15 min at 300g and 4°C. The amount of protein in the supernatant was determined according to Lowry et al. (1951). Lysates with 2-mg ml^{-1} protein were solubilized for 15 min with 1% (w/v) α-DDM on ice in the dark, and insolubilized material was precipitated by centrifugation at 14,000g for 15 min at 4°C. Solubilized material was diluted 1:10 with lysis buffer and incubated for 1 hr at 4°C on an overhead rotator with 50 µl of Protein A-sepharose beads coupled with polyclonal antibodies against HA, HSP22E/F, or pre-immune serum. The coupling of antibodies to Protein A-sepharose was performed as described previously (Schroda et al., 2001). Sepharose beads were washed six times with lysis buffer and twice with 10-mM Tris–HCl, pH 7.0. Proteins were eluted by incubating the samples at 95°C for 5 min in Laemmli buffer lacking DTT. Cells treated with H_2O_2 were washed in lysis buffer (50-mM Hepes-KOH, pH 8, 10-mM KCl, 1-mM MgCl$_2$, 150-mM NaCl), and the cell pellet was frozen with liquid nitrogen and stored at −80°C until lysis. Cells were resuspended in lysis buffer containing 10-mM EGTA, 1 mM PMSF, and 0.5× protease inhibitor cocktail (Roche) and lysed by two passages through a B15 high pressure homogenizer (Avestin) at 900 bar. Lysates were solubilized for 10 min with 1% (w/v) α-DDM on ice, and insolubilized material was removed by centrifugation at 14,000g for 15 min at 4°C. For immunoprecipitations from soluble and membrane fractions, lysis was done in TE buffer with four freeze and thaw cycles. Membrane-enriched fractions were collected by centrifugation. The soluble fraction was supplemented with buffer and salts to match the concentrations employed for the other immunoprecipitations and with 0.1% α-DDM. The membrane pellet was resuspended in the same volume of lysis buffer containing 1% (w/v) α-DDM. Membranes were homogenized by sonication, and the membrane and soluble lysate centrifuged once more for 10 min at 14,000 g and 4°C. Solubilized material was incubated for 1.5 hr at 4°C on an overhead rotator with anti-HA magnetic beads (Pierce), or with Protein A-sepharose beads coupled to antibodies from pre-immune serum or polyclonal antibodies against HSP22E/F and VIPP1. After incubation with the lysate, beads were washed three times with lysis buffer containing 0.1% Tween-20 and three times with lysis buffer without detergent. Proteins were eluted by incubating the samples at 95°C for 1 min in Laemmli buffer lacking DTT. Then, 50-mM DTT was added to the eluates followed by heating for 5 min.

2.11 | Mass spectrometry analysis

Sample preparation and mass spectrometry analysis was performed as described in Müller et al. (2018). In short, immunoprecipitated proteins were supplemented with 0.1-M DTT and allowed to just migrate into the separating gel of an SDS-polyacrylamide gel and stained with colloidal Coomassie G. Protein bands were excised and treated with trypsin before extraction of peptides for analysis by microliquid chromatography tandem mass spectrometry (µLC–MS/MS) using a TripleTOF 6600 instrument coupled to an Eksigent 425 HPLC system (AB SCIEX, Darmstadt). Mass spectrometry data were analysed with the MaxQuant software v1.6.0.1 (Cox et al., 2014; Cox & Mann, 2008) using default

parameters and label-free quantification (LFQ). The *C. reinhardtii* protein database consisted of the JGI v5.5 genome assembly and annotation including mitochondrial and plastid proteins (Rütgers et al., 2017).

3 | RESULTS

3.1 | Gene duplications yielding VIPP paralogs have occurred frequently, but the duplication giving rise to VIPP1 and VIPP2 occurred early during evolution of the green algae

The *C. reinhardtii* genome encodes two VIPP-like proteins termed VIPP1 and VIPP2 (Nordhues et al., 2012). The mature forms of both proteins share 55% identical residues. Other organisms have been reported to contain multiple isoforms of VIPP-like proteins, including cyanobacteria such as *Synechocystis* or *Anabaena* (Kroll et al., 2001) and Gram-positive bacteria such as *Bacillus subtilis* (Manganelli & Gennaro, 2017). Therefore, we wondered whether *Chlamydomonas* VIPP1 and VIPP2 were representatives of two larger, distinct families of VIPP-like proteins. To answer this question, we constructed a phylogenetic tree with 58 sequences of VIPP-like proteins from members of the Archaea, Bacteria (including cyanobacteria), and chloroplast-containing eukaryotes (glaucophytes, diatoms, brown algae, coccolithophores, red algae, and Viridiplantae; Figure 1). The tree revealed that, in addition to cyanobacteria and bacteria, multiple genes encoding VIPP-like proteins can be found frequently in the Viridiplantae (streptophytes and chlorophytes). In contrast, we found no such duplications in the chosen members of the red algae, coccolithophores, brown algae, diatoms, and glaucophytes. All eukaryotic and cyanobacterial VIPP-like sequences can be separated from those of other prokaryotes (proteobacteria, Firmicutes, and Archaea), and all VIPP-like sequences from the Viridiplantae can be separated from those of the other eukaryotic taxa. Hence, *Chlamydomonas VIPP1* and *VIPP2* are both derived from a single *VIPP* gene that existed in the common ancestor of the Viridiplantae. Interestingly, within the chlorophytes, the two VIPP-like sequences from *Chlamydomonas*, *Volvox carteri*, *Dunaliella salina*, and *Chromochloris zofingiensis* form two separate clades, indicating that the duplication that gave rise to VIPP1 and VIPP2 occurred early during the evolution of the green algae.

Westphal et al. (2001) identified a C-terminal extension of about 30 amino acids in VIPPs from cyanobacteria and plants that is absent from bacterial PspA. This extension was therefore suggested to distinguish VIPP from PspA homologues. Indeed, our alignment of the 58 VIPP-like protein sequences (Figure S1) revealed that all sequences from members of the Viridiplantae, red algae, coccolithophores, brown algae, diatoms, and glaucophytes contain this C-terminal extension. Moreover, among the confined cluster of cyanobacterial VIPPs, which can be separated from the cyanobacterial PspA proteins (Figure 1), this C-terminal extension is present, except for the sequence from *Gloeobacter violaceus*. Because this is the only VIPP-like protein encoded by this photosynthetic organism, it is likely to have a similar function to plastid VIPPs. Note, however, that

FIGURE 1   Phylogenetic tree of VIPP-like proteins. The tree is based on the alignment of amino acid sequences of 58 mature VIPP-like proteins. The evolutionary history was inferred using the Neighbor-Joining method. The percentage of replicate trees in which the associated taxa clustered together in the bootstrap test are shown next to the branches. The tree is drawn to scale, with branch lengths in the same units as those of the evolutionary distances used to infer the phylogenetic tree
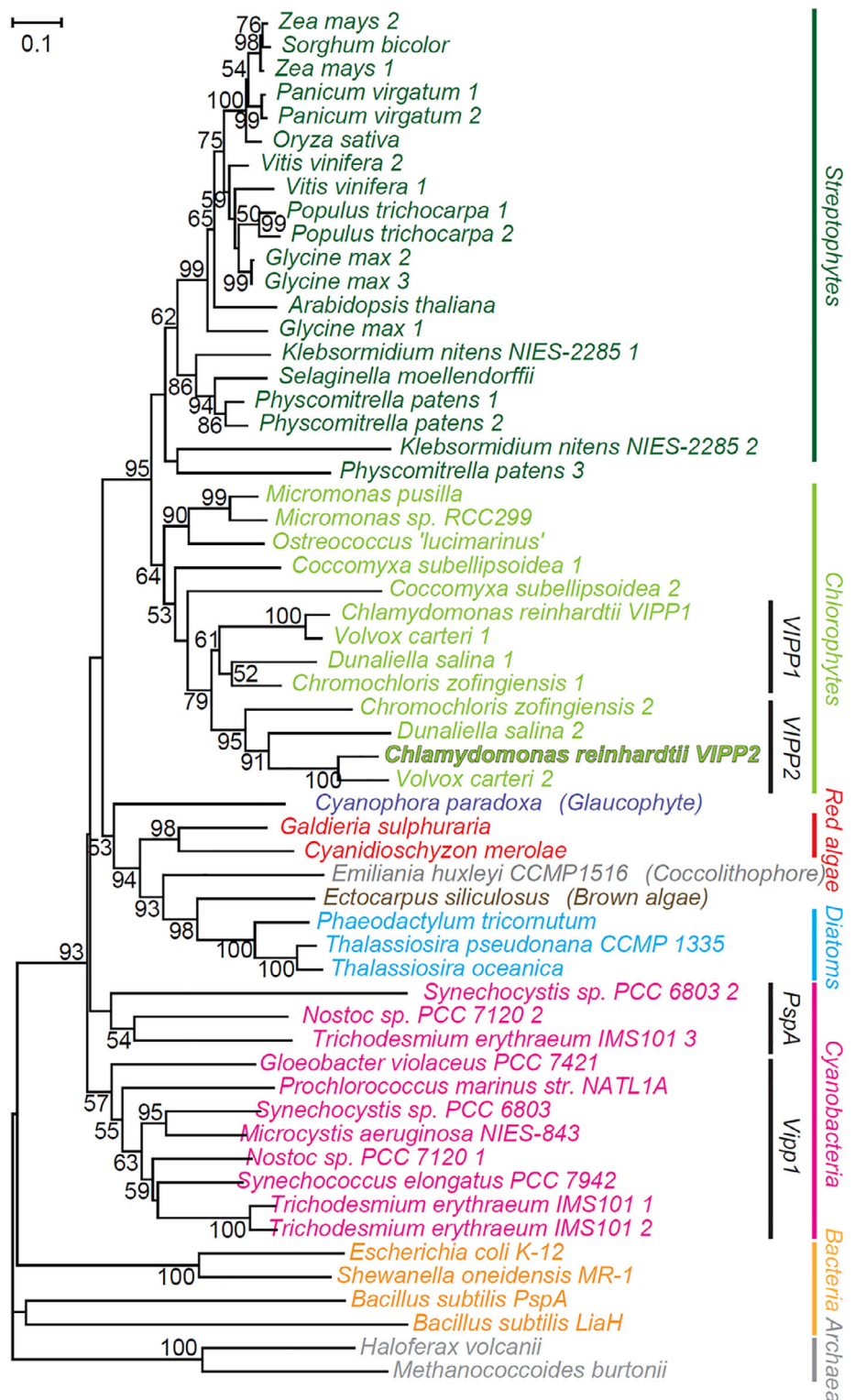
G. violaceus does not contain thylakoids and harbours its photosynthetic complexes in the plasma membrane. Finally, the PspA sequence from *Haloferax volcanii*, a nonphotosynthetic halobacterium, clearly contains the canonical C-terminal extension, as do other PspA proteins in this taxonomic class. Hence, the presence or absence of a C-terminal extension might not be a perfect indicator to assign a given VIPP-like protein to the functional category "PspA" or "VIPP."

3.2 | VIPP2 forms rods in vitro and binds phosphatidylinositol phosphate

To compare the capacity of *Chlamydomonas* VIPP1 and VIPP2 to form oligomers, we expressed both proteins in *Escherichia coli* and purified them to homogeneity (Figure 2a). VIPP2 has 20 more amino acids than VIPP1 (271 versus 251 residues), mainly because of a longer C-terminal
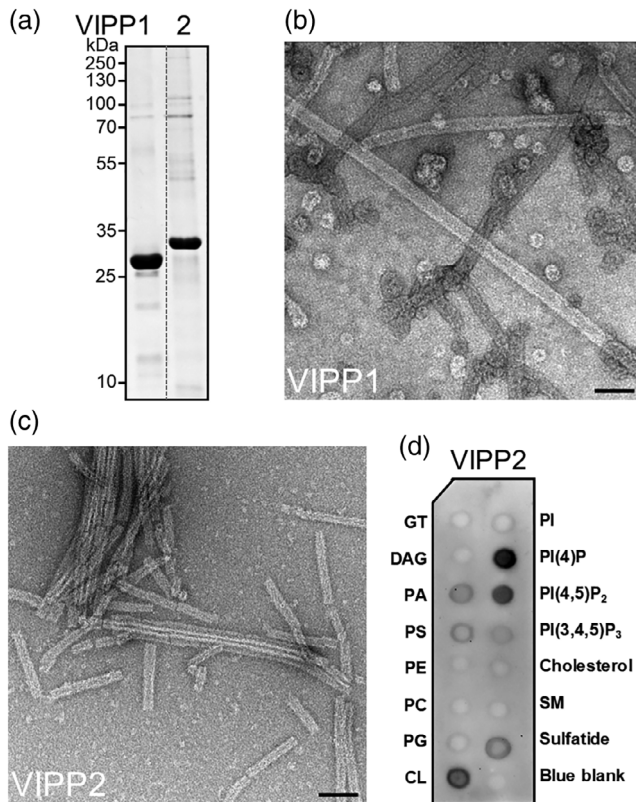
FIGURE 2 Electron micrographs of recombinant *Chlamydomonas* VIPP1 and VIPP2, and lipid binding properties of VIPP2. (a) VIPP1 and VIPP2 lacking their chloroplast transit peptides were produced in *Escherichia coli*. Five micrograms of purified proteins were separated on a 12% SDS-polyacrylamide gel and stained with Coomassie blue. (b) Electron micrograph of purified VIPP1. The black bar corresponds to 0.1 μm. (c) Electron micrograph of purified VIPP2. The black bar corresponds to 0.1 μm. (d) Protein–lipid overlay assay. Membranes with different lipid species spotted were incubated with purified VIPP2 followed by immunodetection of bound protein. Lipid species spotted were GT, glyceryl tripalmitate; DAG, diacylglycerol; PA, phosphatidic acid; PS, phosphatidylserine; PE, phosphatidylethanolamine; PC, phosphatidylcholine; PG, phosphatidylglycerol; CL, cardiolipin; PI, phosphatidylinositol; PIP, phosphatidylinositol phosphate; SM, sphingomyelin. Blue blank (Xylene Cyanol FF) is the negative control

extension (Figure S1). Accordingly, recombinant VIPP2 migrated at ~30 kDa compared with ~28 kDa for VIPP1 in SDS gels (Figure 2a). We examined the purified proteins by negative stain electron microscopy (EM) and could reproduce previous observations that *Chlamydomonas* VIPP1 assembles into ordered rings and rods (Figure 2b; Liu et al., 2007; Theis, Gupta, et al., 2019). VIPP2 was found to predominantly form well-ordered rods, whereas clearly resolved rings were rare (Figure 2c).

VIPP1 was found to interact strongly with phosphatidylinositol phosphates (PIPs; Theis, Gupta, et al., 2019). To test whether this is true also for VIPP2, we subjected recombinant VIPP2 to a lipid overlay assay. As shown in Figure 2d, VIPP2 bound strongest to PI(4)P, and weaker in the following order to PI(4,5)P_2, cardiolipin, sulfatide, phosphatidic acid, and phosphatidylserine.

3.3 | VIPP2 accumulates in cells exposed to HL or H$_2$O$_2$, during recovery from heat stress, and upon impaired transport or integration of thylakoid membrane proteins

VIPP1 and VIPP2 have been shown to accumulate upon exposure of cells to HL intensities (Nordhues et al., 2012; Perlaza et al., 2019). Here, we could verify this result: As shown in Figure 3a, VIPP1 and VIPP2 increasingly accumulated in HL-exposed cells. In contrast to VIPP1, which was clearly detected also under low light (LL) intensities, VIPP2 was detected only upon HL exposure. To ensure that we could distinguish both VIPP paralogs, we ran VIPP1 and VIPP2 on SDS gels next to whole-cell lysate from HL-exposed cells and tested our polyclonal antisera raised against each protein for cross-reactivity. As shown in Figure S2, the antiserum raised against VIPP1 was specific for VIPP1, whereas the antiserum raised against VIPP2 also cross-reacted with VIPP1. Whereas recombinant VIPP1 migrated exactly like the native VIPP1 protein at 28 kDa, native VIPP2 for unknown reasons migrated with a slightly larger apparent mass than recombinant VIPP2, which migrated at 30 kDa. Regardless, we can clearly distinguish VIPP1 from VIPP2 by the different apparent molecular masses, despite the cross-reaction of the VIPP2 antibody with VIPP1.

As H$_2$O$_2$ has been shown to be the major reactive oxygen species (ROS) generated in *Chlamydomonas* cells exposed to 1,000 μmol photons m^{-2} s^{-1} HL conditions (Chang et al., 2014), we tested whether adding H$_2$O$_2$ directly to LL-grown *Chlamydomonas* cells would induce VIPP1/2 expression. As shown in Figure 3b, this was indeed the case. To substantiate these findings, we fused the *VIPP2* promoter (containing 590 bp of sequences upstream of the putative transcriptional start site) or the *βTUB2* promoter (as a control) upstream of the NanoLUC reporter using the MoClo kit (Crozet et al., 2018; Figure 3c). In two independent transformants generated with the *VIPP2::NanoLUC* construct, we found only very weak NanoLUC activity in cells grown in the dark or in LL. However, NanoLUC activity increased on average by a factor of 10 to 16 both under HL conditions and after the addition of H$_2$O$_2$ (Figure 3c), thus corroborating the immunoblot analyses. The transformant with the *βTUB2::* NanoLUC construct showed NanoLUC activity under all conditions, but activity increased with increasing light intensities.

VIPP1 levels have previously been shown to double in cells exposed to heat stress for 24 hr and to remain high during an 8-hr recovery phase (Hemme et al., 2014; Schroda, Hemme, & Mühlhaus, 2015). As VIPP2 was not detected in that study, we analysed VIPP2 levels in cells that had been exposed to heat stress for 2 hr and allowed to recover for another 2 hr (Figure 3d). Interestingly, whereas VIPP1 levels increased during heat stress and remained high during recovery (in line with published results), VIPP2 levels increased only slightly during heat stress, but strongly during the recovery phase.

It has been shown previously that VIPP1 interacts with ALB3.2 and accumulates in *Chlamydomonas* cells when the levels of ALB3.2 have been reduced via RNAi (Göhre, Ossenbuhl, Crevecoeur, Eichacker, & Rochaix, 2006). These findings implicate a role of VIPP1 in facilitating the transport and integration of thylakoid membrane

proteins by ALB3.2 and/or in remedying effects resulting from impaired transport or integration capacities. To extend these findings, we first tested whether the VIPP proteins also accumulated in *ac29*, a mutant lacking the ALB3.1 protein (Ossenbühl et al., 2004). As shown in Figure 3e, *ac29* cells accumulated less LHCII and D1 proteins, thus corroborating the finding that ALB3.1 plays a role in the integration of LHCs and D1 into the thylakoid membrane (Bellafiore, Ferris, Naver, Gohre, & Rochaix, 2002; Ossenbühl et al., 2004). Interestingly, levels of both VIPP1 and VIPP2 were increased in the mutant. Next, we examined a strain harbouring an amiRNA construct under control of the *NIT1* promoter (Schmollinger et al., 2010) that encoded an siRNA targeting the transcript of *SECA*, an essential component of the thylakoid Sec protein translocation system. As shown in Figure 3f, SECA levels were strongly reduced when *SECA*-amiRNA cells had been grown on nitrate-containing TAP medium for 72 hr. At the same time, these cells strongly accumulated VIPP1 and VIPP2. VIPP1 and VIPP2 levels were already slightly elevated in *SECA*-amiRNA cells grown in ammonium-containing TAP medium, presumably because the transgenic *NIT1* promoter was leaky. In cells harbouring an empty amiRNA vector under control of the *NIT1* promoter, the change of the nitrogen source did not lead to increased VIPP levels, ruling out an effect of the nitrogen source. These results extend previous observations by Göhre et al. (2006) and suggest a role of both VIPP proteins in facilitating the transport and integration of thylakoid membrane proteins and/or remedying effects resulting from the disruption of this biogenic process.

3.4 | The accumulation of HSP22E/F in HL is impaired in the *vipp2* mutant

To gain insights into the function of VIPP2, we utilized a strain from the *Chlamydomonas* Library Project (CLiP; Li et al., 2016) harbouring an insertion of the *aphVIII* resistance marker within the third intron of the *VIPP2* gene. By sequencing a PCR product generated from extracted genomic DNA, we confirmed the integration site in the *VIPP2* gene at the 3′ side of the *aphVIII* cassette. At the 5′ side of the cassette, a deletion of ≥1 kb of *VIPP2* genomic DNA appears to have occurred. We base this conclusion on the finding that five PCRs spanning the cassette and sequences 5′ of the integration site failed, whereas three PCRs on the cassette alone were successful (Figure 4a; Figure S3). To further confirm the knock-out, we exposed cultures of two mutant single-clones and a wild-type control to 5 hr of HL and analysed VIPP2 protein levels. VIPP2 strongly accumulated in wild-type cells exposed to HL but was completely absent in both single clones of the *vipp2* insertional mutant (Figure 4b).
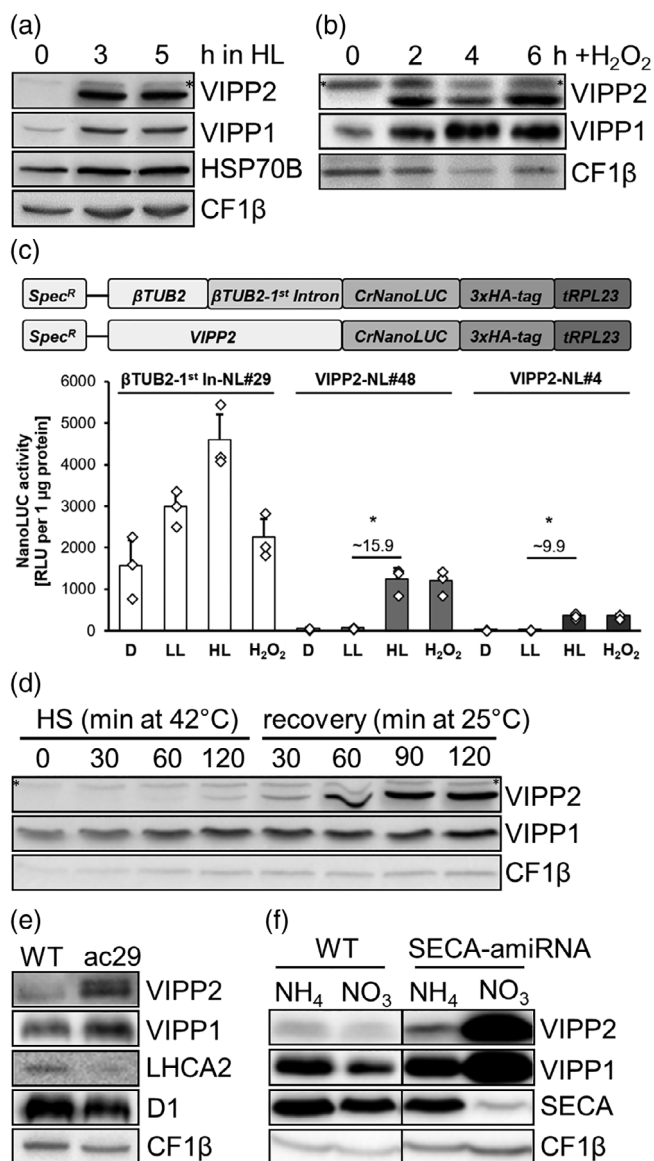

FIGURE 3 Immunoblot analysis of conditions leading to an increased accumulation of VIPP1/2. (a) Exposure of CC-4533 cells to high light (HL) intensities of 800 µmol photons $m^{-2} s^{-1}$ for 5 hr. (b) Incubation of CC-4533 cells with 2-mM H_2O_2 at 30 µmol photons $m^{-2} s^{-1}$ for 6 hr. (c) Analysis of *VIPP2* promoter activity. The promoter and first intron of the *βTUB2* gene or the *VIPP2* promoter were assembled into a level 1 construct with gene parts encoding the NanoLUC reporter (NL), a triple-hemagglutinin (HA) tag, and the 3′UTR of the *RPL23* gene. Level 1 constructs were assembled with an *aadA* cassette (Spec^R) into the shown level 2 constructs. One transformant containing the construct with the *βTUB2* promoter (#29) and two transformants containing the construct with the *VIPP2* promoter (#48 and #4), both in the CF185 background, were grown in the dark for 16 hr (D), continuously in low light at 30 µmol photons $m^{-2} s^{-1}$ (LL), in HL (see (a)), or in the presence of 2 mM H_2O_2 (see (b)). Values indicate fold change of nanoLUC activity of LL compared with HL exposure. Diamonds represent average values of three technical replicates in three independent experiments. Columns represent mean values of the three independent experiments and error bars standard deviations. The significance of differences in nanoLUC activity were determined with a Student's *t* test (**p* < .05). (d) Exposure of cw15-325 cells to heat stress of 42°C (HS) and recovery at 25°C. (e) Analysis of wild-type (WT, cc124) and mutant cells lacking ALB3.1 (*ac29*) grown at a light intensity of 30 µmol photons $m^{-2} s^{-1}$. (f) Growth of cw15-325 cells transformed with an empty amiRNA vector driven by the nitrate reductase promotor (WT) or the same vector containing a siRNA against *SECA* for 72 hr in TAP medium containing ammonia (NH$_4$) or nitrate (NO$_3$)
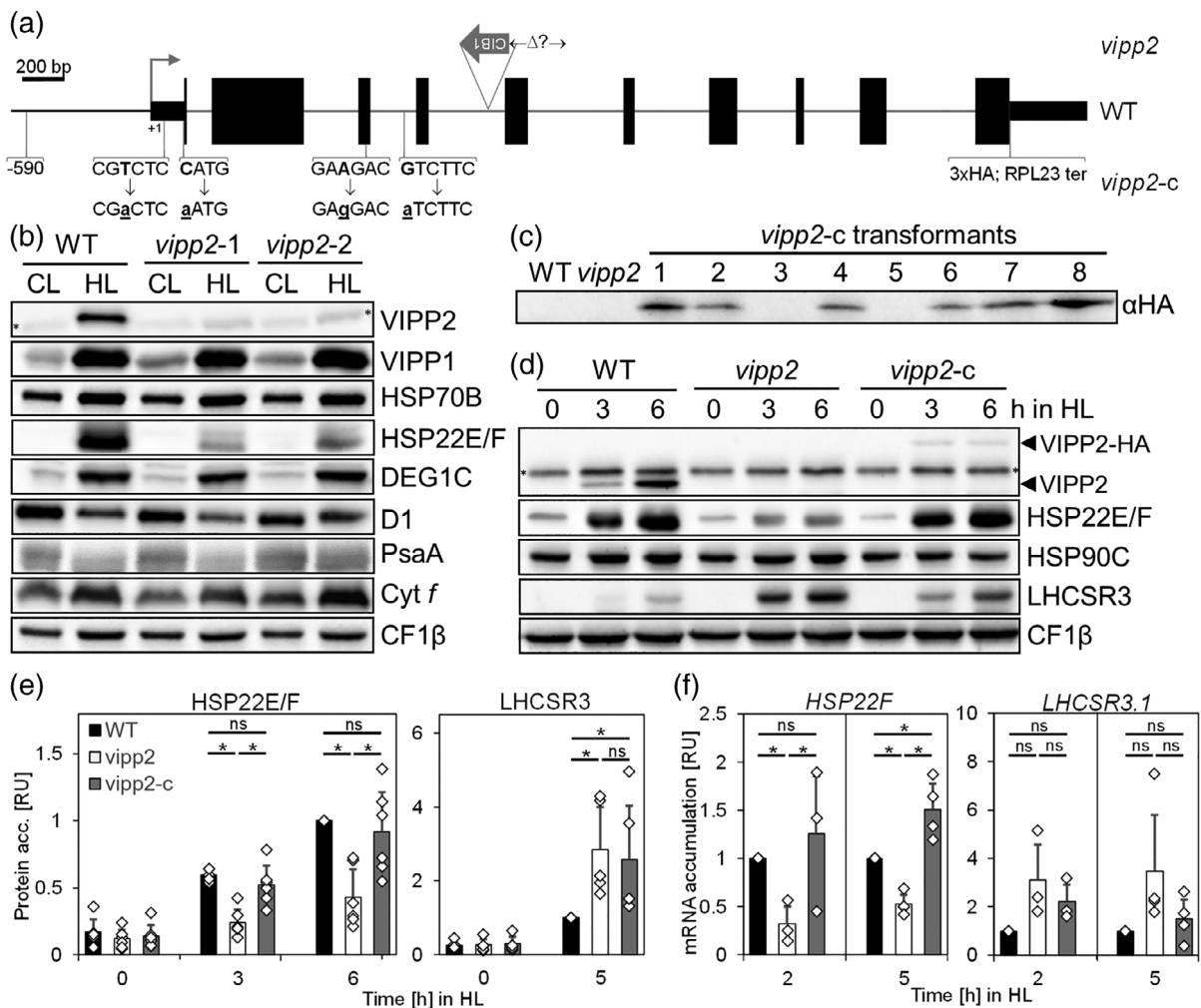
FIGURE 4 Characterization of a vipp2 knock-out mutant and a complemented line. (a) Structure of the VIPP2 nuclear gene. Black lines: promoter sequences; medium black boxes: UTRs; large black boxes: exons; grey lines: introns; thin grey arrow: transcriptional start site. The integration site of the aphVIII cassette with internal barcode (CIB1; Li et al., 2016) and possible deletions of VIPP2 gene sequences in the vipp2 mutant are indicated on top. The construct used for complementation contains 590 bp of VIPP2 upstream regulatory sequences, several silent nucleotide substitutions to domesticate the VIPP2 ORF for the MoClo system, and sequences encoding a triple-HA tag followed by the RPL23 3′ UTR. (b) Analysis of protein accumulation in wild type (CC-4533) and two single clones of the vipp2 mutant line (vipp2-1/2) by immunoblotting. Cells were grown at a light intensity of ~40 μmol m^{-2} s^{-1} (CL) and exposed to 1,000 μmol photons m^{-2} s^{-1} for 5 hr (HL). CF1β served as loading control. The asterisk indicates a protein cross-reacting with the VIPP2 antibody. (c) Immunoblot analysis of CC-4533 (WT), the vipp2 mutant, and transformants generated with vipp2 mutant cells and the construct described in (a) with an antibody against the HA tag. Cells were exposed to 2 mM H$_2$O$_2$ for 5 hr. (d) Analysis of protein accumulation in wild type (CC-4533), vipp2 mutant, and a complemented vipp2 mutant line (vipp2-c) exposed to 800 μmol m^{-2} s^{-1} (HL) for 6 hr by immunoblotting. CF1β served as loading control. (e) Quantification of HSP22E/F and LHCSR3 protein accumulation from six independent HL experiments as shown in (d). Values from each experiment were normalized to protein levels in the wild type reached at the longest HL exposure time. (f) Analysis of transcript accumulation in wild type (CC-4533), vipp2 mutant, and a complemented vipp2 mutant line (vipp2-c) exposed to 800 μmol m^{-2} s^{-1} (HL) for 5 hr by real-time PCR. Diamonds represent average values from three technical replicates from three to four independent experiments. Normalization was done as in (e), but separately for each time point after HL exposure. Error bars represent standard deviations. Significances of differences in protein accumulation were determined with a Student's t test (ns: not significant; *p < .05)

The strong inducibility of VIPP2 under HL exposure indicates a HL-specific function for this protein, and thus phenotypes in the vipp2 mutant are likely to appear in HL. We therefore monitored the accumulation of VIPP1, proteins involved in chloroplast protein quality control, and components of the photosynthetic light reactions in the HL-exposed vipp2 mutant. Interestingly, the HL-induced accumulation of HSP22E/F was strongly impaired in both single clones of the vipp2

mutant, whereas we found no differences between wild-type and vipp2 cells regarding the HL-induced accumulation of VIPP1, HSP70B, DEG1C, cytochrome f, and CF1β. Neither did we observe differences in the HL-induced decrease in levels of D1 and PsaA (Figure 4b).

We used the MoClo strategy (Crozet et al., 2018) to generate a construct for complementing the vipp2 mutant. Six out of eight spectinomycin-resistant transformants analysed expressed the

VIPP2-HA fusion protein after exposure to H_2O_2 and were termed *vipp2-c* (Figure 4c). Next, we tested whether the impaired accumulation of HSP22E/F in HL-exposed *vipp2* mutant cells could be restored in *vipp2-c* cells. For this, we exposed wild-type, *vipp2* mutant, and *vipp2-c* cells to 6 hr of HL and used the VIPP2 antibody to quantify how much VIPP2 protein accumulated in *vipp2-c* cells compared with wild-type cells (Figure 4d). The *vipp2-c* cells contained 31% ± 7% (*SD*, *n* = 3) and 9% ± 1% (*SD*, *n* = 3) of wild-type VIPP2 levels after 3 and 6 hr in HL, respectively. Despite these rather modest VIPP2 expression levels, *vipp2-c* cells fully restored the ability to accumulate HSP22E/F upon HL exposure (Figure 4d,e).

The LHCSR3 protein accumulates in *Chlamydomonas* cells exposed to HL and is required for nonphotochemical quenching (Allorent & Petroutsos, 2017; Peers et al., 2009). As the accumulation of the LHCSR3 protein has been shown to be impaired in HL-exposed *VIPP1*-RNAi lines (Nordhues et al., 2012), we also tested LHCSR3 levels in HL-exposed *vipp2* mutant and *vipp2-c* cells. Surprisingly, the *vipp2* mutant accumulated LHCSR3 to higher levels than wild-type cells, but this phenotype was not fully restored in *vipp2-c* (Figure 4d and Figure 4e). To test whether the impaired accumulation of HSP22E/F and the increased accumulation of LHCSR3 was caused by altered gene expression or altered protein stability, we analysed transcript levels in HL-exposed wild-type, *vipp2* mutant, and *vipp2-c* cells. As shown in Figure 4f, *HSP22F* transcript levels in cells exposed to HL for 2 or 5 hr were lower in the *vipp2* mutant than in wild type, and this was reverted in the complemented line. *LHCSR3* transcript levels in cells exposed to HL for 2 or 5 hr were higher in the *vipp2* mutant than in wild type, and there was a trend that this also was reverted in the complemented line. These data indicate a role of VIPP2 in regulating retrograde signalling that controls the expression of the *HSP22E/F* and *LHCSR3* genes.

3.5 | VIPP2 is predominantly present in membrane fractions, whereas VIPP1 is more evenly distributed between both

The HA-tagged VIPP2 protein in the *vipp2-c* lines allowed us to specifically detect VIPP2 with an HA antibody, thus avoiding cross-reactivity of the VIPP2 antibody with VIPP1 (Figure S2). We took advantage of the HA tagging to localize VIPP2 within the cell by immunofluorescence. As shown in Figure 5a, the HA antibody gave hardly any signal in HL-exposed wild-type cells but a strong signal in HL-exposed *vipp2-c* cells. There, VIPP2 was detected in the chloroplast and was occasionally enriched in broad punctae. In comparison, chloroplast-resident HSP70B was detected in both wild-type and *vipp2-c* cells with a more diffuse localization pattern.

VIPP1 has been shown to localize to both the stroma and chloroplast membranes in *Chlamydomonas* (Liu et al., 2005). To test whether this holds true also for VIPP2, we fractionated LL-grown cells that had been supplemented for 4 hr with 2 mM H_2O_2 by freezing and thawing followed by centrifugation. As judged from the presence of on
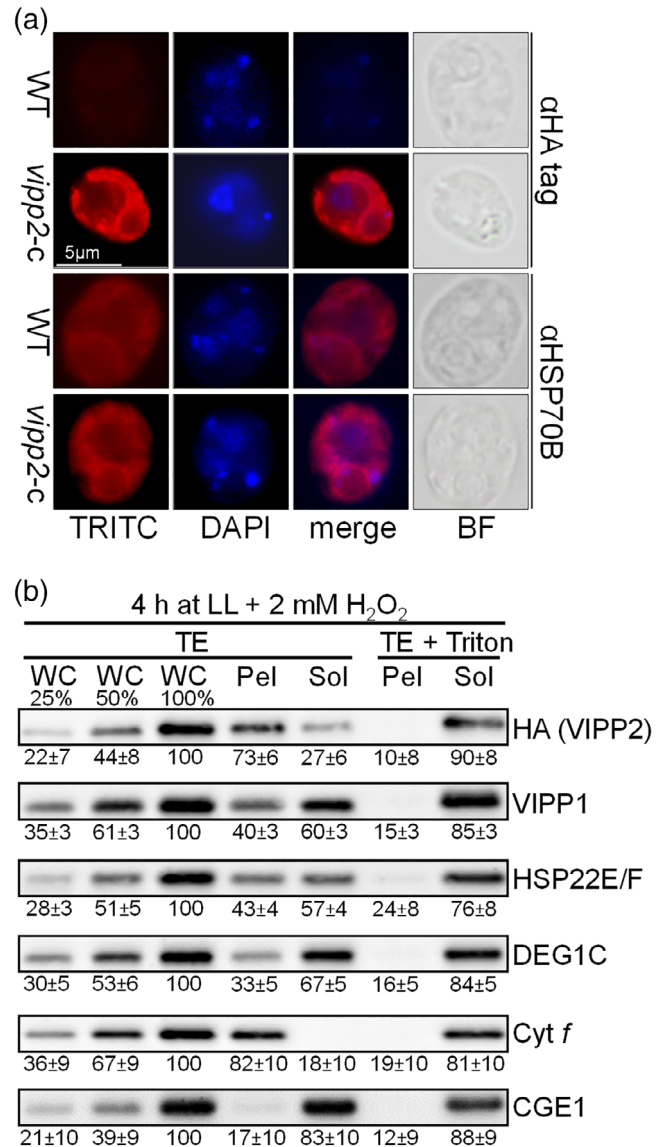

FIGURE 5 Intracellular localization of VIPP2 in relation to other chloroplast proteins. (a) Intracellular localization of VIPP2-HA by immunofluorescence microscopy. Images were taken from cells of CC-4533 (WT) and a complemented *vipp2* mutant line (*vipp2-c*) exposed to 800 μmol m^{-2} s^{-1} for 5 hr. Shown are from left to right: immunofluorescence using antibodies against the HA tag and chloroplast-resident HSP70B (TRITC), DAPI staining, the merge of DAPI and TRITC, and bright field (BF) images. (b) Localization of VIPP2, VIPP1, HSP22E/F, and DEG1C to cell fractions. After exposure to H_2O_2 for 4 hr, *vipp2-c* cells were resuspended in Tris-EDTA (TE) buffer lacking or containing 2% Triton X-100, subjected to three cycles of freezing/thawing followed by centrifugation. Whole cells (WC), pellet (Pel), and soluble (Sol) fractions were loaded on the basis of equal volumes and analysed by immunoblotting. Soluble stroma protein CGE1 and intrinsic thylakoid membrane protein cytochrome *f* served as controls. Values given below the immunoblots indicate the averages and standard deviations of band intensities from three biological replicates. For WC proteins, 25%, 50%, and 100% were loaded and quantified values normalized to the 100% signal. Values for fractions are the percentage of the sum of signals from soluble and pellet fractions

average ~83% of stromal CGE1 in the soluble fraction and ~82% of membrane-intrinsic cytochrome *f* in the pellet fraction, this procedure reliably separates soluble proteins from membrane proteins (Figure 5b). Corroborating earlier findings, ~40% of VIPP1 was detected in the pellet and ~60% in the soluble fraction. In contrast, ~73% of VIPP2 was in the pellet and only ~27% in the soluble fraction (Figure 5b).

As HSP22E/F expression is modulated by VIPP2 (Figure 4), we also monitored the fractionation pattern of HSP22E/F. Strikingly, it resembled that of VIPP1, with ~43% of HSP22E/F present in the pellet and ~57% in the soluble fraction. We included DEG1C in our analysis, the major chloroplast Deg-type protease that localizes to the stroma and thylakoid membranes (Theis, Lang, et al., 2019). Compared with VIPP2, HSP22E/F, and VIPP1, a lower percentage of DEG1C was found in the pellet fraction (~33%; Figure 5b).

Because VIPP1 and VIPP2 can both form large rods in vitro (Figure 2), it is possible that they localized to the pellet fraction because of their size and not because they are associated with membranes. We therefore repeated the fractionation experiment in the presence of 2% Triton X-100. Like for CGE1, >80% of cytochrome *f* was now recovered in the soluble fraction, indicating complete solubilization of thylakoid membranes (Figure 5b). Similarly, >80% of VIPP2, VIPP1, and DEG1C were now in the soluble fraction. This indicates that, in the absence of detergent, these proteins fractionate to the pellet because they are membrane associated in vivo, and not because they form large oligomers or aggregates. A little less of HSP22E/F was recovered in the soluble fraction (~76%), indicating that some HSP22E/F might exist in larger aggregates.

3.6 | The *vipp2* mutant behaves like wild type regarding photoautotrophic growth and the ability to recover PSII activity after photoinhibition or sulphur starvation

Chlamydomonas VIPP1-RNAi lines were previously reported to be impaired in the biogenesis and repair of photosystem II (PSII;

Nordhues et al., 2012). This prompted us to investigate possible phenotypes of the *vipp2* mutant related to photoautotrophic growth as well as PSII biogenesis and repair. Spot tests revealed no differences between wild type and the *vipp2* mutant in mixotrophic and photoautotrophic growth (Figure S4a). We then exposed wild-type and *vipp2* mutant cells to photoinhibitory light for 1 hr in the presence of chloramphenicol (to block PSII repair) and found no differences in the extent of loss of PSII maximum quantum efficiency (Figure S4b). After washing out chloramphenicol and placing cultures into LL for 5 hr to allow PSII repair to take place, we found no difference in the rate at which PSII maximum quantum efficiency recovered. Hence, the sensitivity to HL and the ability to repair PSII are not affected in the *vipp2* mutant. Next, we depleted sulphur from wild-type and *vipp2* mutant cultures for 48 hr in LL to induce the degradation of PSII and repleted the cultures with sulphur for another 18 hr to allow PSII de novo biogenesis to take place (Muranaka et al., 2016). As shown in Figure S4c, PSII degradation and recovery were indistinguishable between wild type and the *vipp2* mutant, suggesting that VIPP2 plays a role in neither PSII degradation nor PSII biogenesis.

3.7 | VIPP2 interacts with VIPP1 as major partner and with HSP22E/F as minor partner

To identify proteins interacting with VIPP2, we exposed wild-type and *vipp2*-c cells to HL for 5 hr, solubilized the cells with n-dodecyl α-D-maltoside (α-DDM), and performed immunoprecipitations with an HA antibody. Immunoprecipitated proteins were then analysed by mass spectrometry (IP-MS). In four independent immunoprecipitates (each measured twice), we identified a total of 125 proteins that were detected at least once. We looked for proteins that were not detected in wild-type cells but detected in at least two precipitates from *vipp2*-c cells with at least two unique peptides. Only three of the 125 proteins fulfilled these criteria, which were VIPP2 itself, VIPP1, and HSP22E/F. We considered HSP22E and HSP22F as a single entity because the mature proteins lacking chloroplast transit peptides differ by only eight amino acids (Rütgers et al., 2017), and thus mass

TABLE 1 Proteins found in αHA immunoprecipitates from α-DDM solubilized wild-type and *vipp2*-c cells exposed to HL

Gene ID	Name	Unique peptides	Protein coverage	Summed ion intensities WT control (×1000)				Summed ion intensities VIPP2-HA (×1000)			
				Exp1	Exp2	Exp3	Exp4	Exp1	Exp2	Exp3	Exp4
Cre11.g468050	VIPP2	19	72.0%	0	0	0	0	42.8	48.5	58.1	58.9
Cre13.g583550	VIPP1	12	51.4%	0	0	0	0	17.6	17.3	20.6	19.2
Cre14.g617450/ Cre14.g617400	HSP22E/F	4	26.3%	0	0	0	0	3.3	2.7	*3.0*	3.2

Note: Values for summed ion intensities (LFQ values from the MaxQuant software) are the mean of two LC–MS/MS runs on the same sample. Samples came from four independent immunoprecipitation experiments (Exp1–4). Italicized values indicate that ion intensity values were retrieved from only one LC–MS/MS run on the same sample. Protein coverage refers to the protein without chloroplast transit peptide. Among 125 detected proteins, only those that are absent in all control samples and were detected with ≥2 unique peptides in ≥2 experiments are shown. The positions of identified peptides within the proteins are shown in Figure S5, all LC–MS/MS data are provided in Table S2.
Abbreviations: HL, high light; LC–MS/MS, liquid chromatography tandem mass spectrometry; LFQ, label-free quantification.

spectrometry could not distinguish between the two proteins. All three proteins were detected in all experiments with a total of 4–19 unique peptides (Table 1; Table S2; Figure S5). On the basis of summed ion intensities, VIPP2 was 2.8-fold more abundant than VIPP1 and 17.1-fold more abundant than HSP22E/F in the precipitates, implicating VIPP1 as a major interaction partner and HSP22E/F as a minor interaction partner of VIPP2.

To verify these results, we first repeated the immunoprecipitation on α-DDM solubilized, HL-exposed wild-type and $vipp2$-c cells using the HA antibody. As shown in Figure 6a, small amounts of HSP22E/F were indeed detectable in the precipitate from $vipp2$-c cells, but not in the precipitate from wild-type cells. In a reciprocal experiment, we used the antibody against HSP22F and preimmune serum as a control to immunoprecipitate HSP22E/F from $vipp2$-c cells. Slightly higher quantities of VIPP2 were detected in precipitates generated with the HSP22F antibody than in precipitates generated with preimmune serum (Figure 6a).

We conducted the same experiment with wild-type and $vipp2$-c cells exposed to 2-mM H_2O_2 for 4 hr and included VIPP1 in the analysis. Again, small amounts of HSP22E/F were detected in the precipitate generated with the HA antibody on $vipp2$-c cells, but not in the precipitate generated from wild-type cells (Figure 6b). Compared with HSP22E/F, much more VIPP1 was found in the precipitate generated with the HA antibody on $vipp2$-c cells, whereas no VIPP1 was found in the precipitate from wild-type cells. These results mirror the IP-MS data. In the reciprocal experiment, using the antibody against HSP22F for immunoprecipitation, we detected neither VIPP2 nor VIPP1. Presumably, HA-tagged VIPP2 is much less abundant than HSP22E/F, and a greater fraction of the VIPP2 pool interacts with HSP22E/F than vice versa. However, when using the VIPP1 antibody for immunoprecipitation, we could detect small amounts of VIPP2 in the precipitate generated from $vipp2$-c cells but not in the precipitate from wild-type cells (Figure 6b). No HSP22E/F above background levels could be coprecipitated with VIPP1.

As VIPP2 is found predominantly in membrane-enriched fractions (Figure 5b), we wondered whether the interaction of VIPP2 with VIPP1 and HSP22E/F also occurred predominantly at membranes. To this end, we prepared soluble and membrane-enriched fractions from wild-type and $vipp2$-c cells exposed to 2-mM H_2O_2 for 4 hr and immunoprecipitated HA-tagged VIPP2. In this experiment, only ~8% of VIPP2 was detected in soluble fractions, and ~92% was in membrane-enriched fractions (Figure 6c). More VIPP2 (~28%) was recovered in immunoprecipitates from soluble fractions, presumably because HA-antibody binding sites got saturated in the immunoprecipitations on membrane-enriched fractions. The opposite was observed for VIPP1 and HSP22E/F: Here, more VIPP1 (~79% versus ~56%) and more HSP22E/F (~83% versus ~54%) were found in the VIPP2 immunoprecipitates from membrane-enriched fractions when compared with soluble fractions. This indicates that interactions of VIPP2 with VIPP1 and HSP22E/F preferably take place at chloroplast membranes. We also detected the chloroplast HSP70B chaperone as a control and found it to specifically coprecipitate with VIPP2, but preferably in the soluble fractions. The specific coprecipitation of
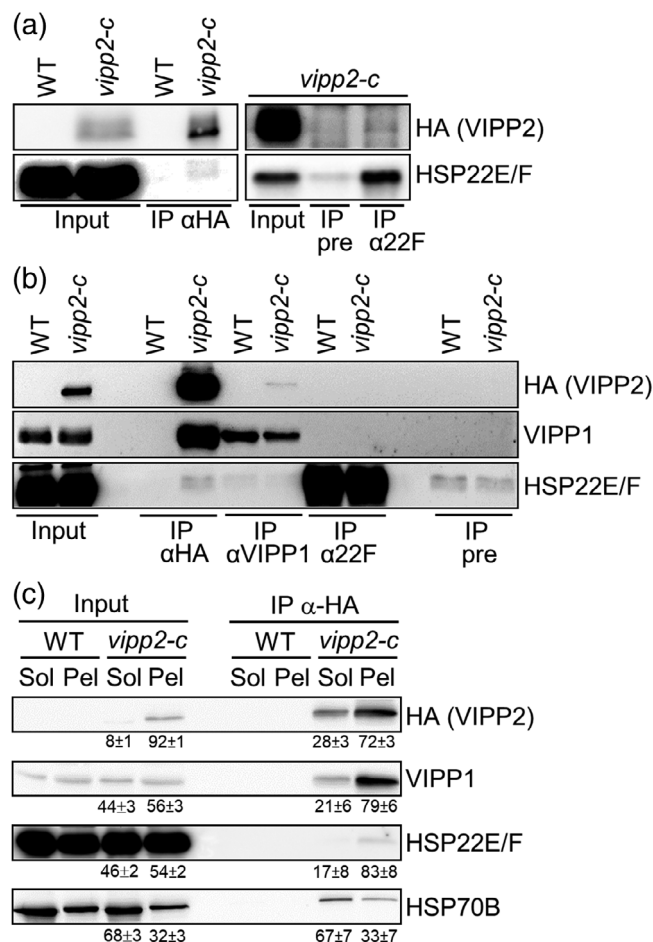

FIGURE 6 Verification of VIPP2 interaction partners. (a) Immunoblot analysis of immunoprecipitates (IP) generated with antibodies against the HA tag, HSP22F, and with preimmune serum (pre) on wild type (WT, CC-4533) and the complemented $vipp2$ mutant expressing HA-tagged VIPP2 ($vipp2$-c). Cells were exposed to 800 µmol photons m^{-2} s^{-1} for 5 hr and solubilized with 1% α-DDM. (b) Immunoblot analysis of IPs generated with the same antibodies as in (a) plus the VIPP1 antibody on wild type and $vipp2$-c exposed to 2 mM H_2O_2 for 4 hr and solubilized with 1% α-DDM. (c) Immunoblot analysis of IPs on cell fractions. Wild type (WT) and $vipp2$-c were exposed to 2 mM H_2O_2 for 4 hr and subjected to four cycles of freezing/thawing followed by centrifugation to generate fractions enriched in soluble (Sol) and membrane (Pel) proteins. The fractions were resuspended in equal volumes and supplemented with 1% α-DDM (membrane) or 0.1% α-DDM (soluble) and subjected to immunoprecipitation using an antibody against the HA tag. Values given below the immunoblots indicate the averages and standard deviations of band intensities from three biological replicates. They represent the percentage of the sum of signals from soluble and pellet fractions

HSP70B is surprising, because in the IP-MS experiment, HSP70B was not specifically coprecipitated with HA-tagged VIPP2 (Table S2). We attribute this to the difference that we used Protein A-sepharose coupled to the HA antibody in the IP-MS experiments but anti-HA magnetic beads in the experiment shown in Figure 6c. In our hands, HSP70s tend to stick to Protein A-sepharose, and this may have concealed specific binding of HSP70B to VIPP2.

4 | DISCUSSION

We report here on VIPP2, one of two VIPPs encoded by the *Chlamydomonas* genome, which share 55% sequence identity. Phylogenetic analyses on VIPP-like proteins revealed that duplications of *VIPP* genes have occurred frequently and rather recently in the Viridiplantae, but the duplication giving rise to the VIPP1 and VIPP2 paralogs took place early during the evolution of the green algae (Figures 1 and S1).

4.1 | Shared and distinct properties of VIPP1 and VIPP2

Chlamydomonas VIPP1 and VIPP2 have several properties in common. They share that their expression is induced in HL (Figure 3a; Nordhues et al., 2012; Perlaza et al., 2019), after the addition of H_2O_2 (Figure 3b), upon depletion of the chloroplast proteases ClpP and DEG1C (Perlaza et al., 2019; Ramundo et al., 2014; Theis, Lang, et al., 2019), and when the translocation or integration of thylakoid membrane proteins is impaired (Figure 3d,e; Göhre et al., 2006). VIPP1 and VIPP2 also share the ability to form rod-like structures in vitro (Figure 2b,c; Liu et al., 2007; Theis, Gupta, et al., 2019). Finally, both VIPP2 and VIPP1 interact with the chloroplast HSP70B chaperone (Figure 6c), which, at least in the case of VIPP1, plays a role in controlling its oligomeric state (Liu et al., 2005; Liu et al., 2007).

Several other features distinguish the two proteins from each other. VIPP1 is constitutively expressed, whereas VIPP2 is barely expressed under ambient conditions (Nordhues et al., 2012; Perlaza et al., 2019). Levels of both proteins rise mildly during heat stress, but whereas VIPP1 levels remain stable during the recovery from heat stress (Hemme et al., 2014), VIPP2 levels increase strongly (Figure 3c). Another difference is that VIPP2 is predominantly found in membrane fractions of H_2O_2-exposed cells, whereas VIPP1 is about equally distributed between soluble and membrane fractions (Figures 5b and 6c). Finally, VIPP2 has a different lipid binding preference than VIPP1. VIPP2 bound strongest to phosphatidylinositol-4-phosphate (PI(4)P) and weaker in the following order to PI(4,5)P$_2$, cardiolipin, sulfatide, phosphatidic acid, and phosphatidylserine (Figure 2d). In contrast, VIPP1 bound strongest to PI(3,4,5)P$_3$ and PI(4,5)P$_2$, weaker to PI(4)P, and not at all to any of the other lipids bound by VIPP2 (Theis, Gupta, et al., 2019).

Perhaps the most important difference between the two proteins is that *Chlamydomonas* VIPP1 knock-down lines showed severe defects, including impaired biogenesis and repair of PSII and a higher sensitivity of PSII to HL and heat stress (Nordhues et al., 2012). In contrast, the *vipp2* knock-out line behaved like wild type regarding the sensitivity of PSII to HL and the ability to synthesize and repair PSII (Figure S4). Finally, VIPP1 appears to act positively on the HL-induced expression of *LHCSR3*, because *LHCSR3* gene expression was reduced in *vipp1* knock-down lines (Nordhues et al., 2012). In contrast, VIPP2 appears to act negatively on *LHCSR3* gene expression, as the HL-induced expression of LHCSR3 was increased in *vipp2* knock-out lines (Figure 4d–f). However, as the LHCSR3 overaccumulation phenotype was only slightly reduced in complemented *vipp2* mutant lines that express VIPP2 to 9–31% of wild-type

levels, we cannot say whether this incomplete rescue was due to the weak expression of VIPP2 or because the LHCSR3 phenotype is caused by a defect in the *vipp2* mutant that is unrelated to the *vipp2* knock-out.

4.2 | VIPP1 appears to be sufficient to cover the demand for VIPP-like proteins for the biogenesis and repair of major protein complexes in thylakoid membranes

Many functions have been assigned to VIPP proteins in various organisms that perform oxygenic photosynthesis. Generally, these functions can be grouped into two categories: (a) the biogenesis and repair of major protein complexes in thylakoid membranes (Aseeva et al., 2007; Fuhrmann, Gathmann, et al., 2009; Gao & Xu, 2009; Gutu et al., 2018; Kroll et al., 2001; Nordhues et al., 2012; Walter et al., 2015; Westphal et al., 2001; Zhang et al., 2014; Zhang & Sakamoto, 2013) and (b) coping with chloroplast membrane stress (Zhang et al., 2012; Zhang, Kondo, et al., 2016; Zhang, Kusaba, et al., 2016).

We previously proposed the idea that VIPP1 might be able to organize domains in chloroplast membranes that resemble eisosomes found in fungal plasma membranes (Rütgers & Schroda, 2013; Theis, Gupta, et al., 2019; Theis & Schroda, 2016). Such membrane domains may attract translocases such as TAT and SEC as well as integrases like ALB3 while providing a lipid environment that is essential for their proper function. This would explain how VIPP-like proteins aid in protein translocation across and protein integration into membranes and thereby VIPP1's role in supporting the biogenesis of thylakoid membrane protein complexes (DeLisa, Lee, Palmer, & Georgiou, 2004; Göhre et al., 2006; Lo & Theg, 2012; Vrancken et al., 2007; Walter et al., 2015). In *Chlamydomonas* grown under ambient conditions, VIPP1 alone appears to cover the demand for VIPP-like proteins for the de novo biogenesis of thylakoid membrane protein complexes, because VIPP2 is barely expressed under these conditions and PSII de novo biogenesis was unaffected in the *vipp2* knock-out mutant (Figure S4c). Nevertheless, VIPP2 can replace VIPP1 in this role, as thylakoid membrane protein complexes were made when VIPP1 was depleted to <5% of wild-type levels and VIPP2 was upregulated to ~20% of normal VIPP1 levels (Nordhues et al., 2012). The lack of VIPP1 in Arabidopsis leads to a complete loss of thylakoid membranes (Zhang et al., 2012). Additionally, a possible demand for VIPP-like proteins during PSII repair apparently can be fulfilled by VIPP1 alone, as we did not detect any impairment of the PSII repair capacity in the *vipp2* mutant (Figure S4b). Hence, if the concept of thylakoid membrane domains for biogenesis and repair processes is correct, such domains apparently can be organized largely by VIPP1. What then might be the function of VIPP2?

4.3 | VIPP2 may play a role in the sensing of membrane lipid-packing defects, presumably via its N-terminal amphipathic α-helix

Membrane lipid-packing defects can be caused by the accumulation of misfolded and unassembled membrane proteins (McDonald et al.,

2015), for example, when components of translocases/integrases like SECA or ALB3 are missing (Figure 3e,f; Göhre et al., 2006), when levels of clearing proteases such as ClpP or DEG1C are reduced (Perlaza et al., 2019; Ramundo et al., 2014; Theis, Lang, et al., 2019), or when membrane proteins misfold because they get oxidized by ROS generated in HL. Membrane lipid-packing defects may also arise from direct effects on the properties of the lipid bilayer inflicted by ROS-mediated lipid peroxidation (Wong-Ekkabut et al., 2007; Zhang, Kusaba, et al., 2016), rapid changes in membrane viscosity upon a sudden drop in temperature (Figure 3c; Zhang, Kondo, et al., 2016), or osmotic stress (Zhang et al., 2012). All of these conditions have in common that they force lipids in one leaflet of the membrane bilayer to adopt an unfavourable packing conformation, thereby generating stored curvature elastic (SCE) stress in the bilayer (McDonald et al., 2015).

SCE stress is thought to produce hydrophobic cavities within the membrane into which amphipathic α-helices can insert (Attard, Templer, Smith, Hunt, & Jackowski, 2000). Recent pioneering work has revealed that the N-terminal 24 amino acids of VIPP-like proteins form such an amphipathic α-helix (AHa) that mediates membrane binding upon oligomerization of the proteins (Jovanovic et al., 2014; McDonald et al., 2015; McDonald et al., 2017; Otters et al., 2013). The major determinant for membrane binding is the extent of SCE stress, and a minor determinant is the presence of anionic lipids. Notably, the SCE stress-dependent AHa binding is much more apparent for *E. coli* PspA, whereas *Synechocystis* VIPP1 membrane association is more strongly modulated by anionic lipids. This was explained by the higher hydrophobicity of the nonpolar face of PspA's AHa and the greater number of cationic residues in the polar face of VIPP1's AHa (McDonald et al., 2015; McDonald et al., 2017).

When we compare the physicochemical properties of the AHa domains in VIPP1 and VIPP2 from Chlorophyceae members *C. reinhardtii*, *V. carteri*, *D. salina*, and *C. zofingiensis*, we find 2-3 substitutions of Ala/Ser in VIPP1 to Phe/Val in VIPP2 in the nonpolar face (Figures 7 and S6; Gautier, Douguet, Antonny, & Drin, 2008). This indicates that VIPP2 might have a higher affinity for membranes experiencing SCE stress, whereas VIPP1's affinity for membranes might depend more on anionic lipids. This is consistent with the proposed role of VIPP1 in the biogenesis and repair of thylakoid membrane protein complexes and also consistent with the higher affinity of VIPP1 for poly-phosphorylated PIPs when compared with VIPP2 (Theis, Gupta, et al., 2019; Figure 2d). A role for VIPP2 in sensing membrane stress is supported by the findings that VIPP2 is predominantly found in membrane fractions of H_2O_2-treated cells, where it interacts with VIPP1 and HSP22E/F (Figures 5b and 6c), and that VIPP2 modulates the expression of nuclear genes *HSP22E/F* and *LHCSR3*, most likely via a retrograde signal (Figure 4). Interestingly, values for hydrophobicity and/or hydrophobic moment for the AHa from *Arabidopsis* VIPP1 lie between those for VIPP1 and VIPP2 from the Chlorophyceae (Figures 7 and S6). This might explain why *Arabidopsis* VIPP1 is apparently more multifunctional, aiding in both the coping with membrane stress and the biogenesis and repair of thylakoid protein complexes, whereas specialization took place in the
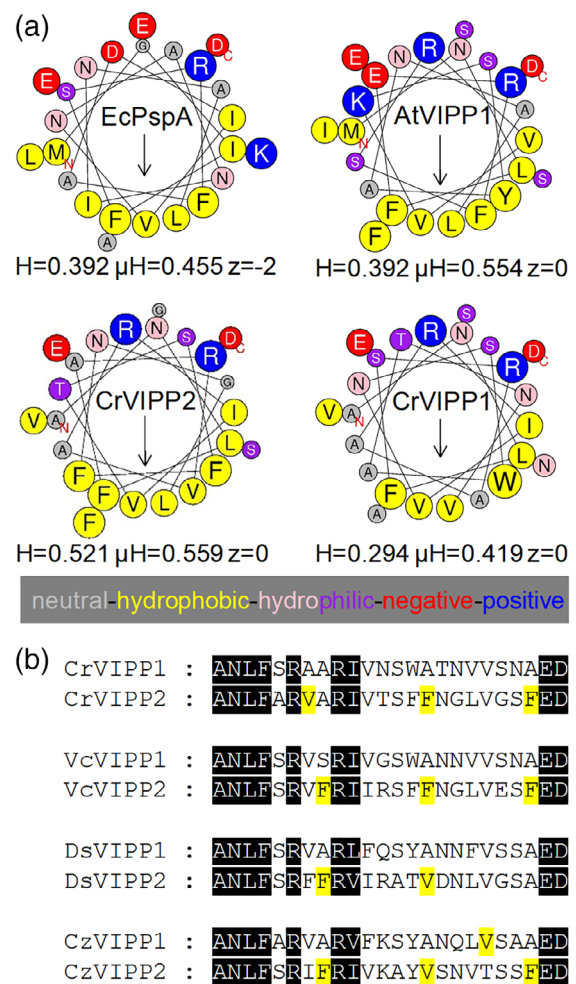

FIGURE 7 Comparison of amphipathic α-helices (AHa) of VIPP-like proteins. (a) Helical-wheel projections of the N-terminal 24 amino acids constituting the AHa domain of VIPP-like proteins that mediate membrane binding. The physicochemical parameters of hydrophobicity (H), hydrophobic moment (μH), and net charge (z) are given below each projection. Projections and calculations were made with HELIQUEST (Gautier et al., 2008). Arrows within each projection show the direction of μH. Ec, *Escherichia coli*; At, *Arabidopsis thaliana*; Cr, *Chlamydomonas reinhardtii*. (b) Alignment of amino acids constituting the AHa domain of VIPP1 and VIPP2 orthologs from different members of the Chlorophyceae. Vc, *Volvox carteri*; Ds, *Dunaliella salina*; Cz, *Chromochloris zofingiensis*. Amino acids shaded in black are conserved in all eight VIPP1/2 sequences. Letters shaded in yellow indicate positions where neutral Ala or hydrophilic Ser/Thr were substituted by hydrophobic Phe or Val

Chlorophyceae. By oligomerizing with VIPP1 under stress conditions, VIPP2 might increase the affinity of VIPP1-VIPP2 heterooligomers to sites of membrane lipid-packing defects. However, the quantity of VIPP1 recruited by VIPP2 to such sites is expected to be low: Quantitative immunoblotting revealed that VIPP2 accumulates to at most 20% of the levels to which VIPP1 accumulates (Nordhues et al., 2012). After 4 hr of H_2O_2 treatment, ~73% of the VIPP2 pool localized to membranes (Figure 5b). VIPP2 at membranes formed heterooligomers with VIPP1 in which VIPP2 was ~2.8-fold more

abundant than VIPP1 (Table 1). On the basis of these considerations, VIPP2 would recruit only ~5% of the cellular VIPP1 pool to sites of membrane lipid-packing defects under HL/H_2O_2 stress. In line with these considerations, in cells exposed to H_2O_2 for 4 hr, we observed a trend for slightly decreased partitioning of VIPP1 to membrane fractions in the *vipp2* mutant compared with wild type, which reverted in the complemented line (Figure S7).

4.4 | VIPP1/2 may function together with HSP22E/F to prevent and recover from chloroplast membrane stress

VIPP2 interacted with both VIPP1 and HSP22E/F in *Chlamydomonas* cells exposed to HL or H_2O_2, and this interaction took place predominantly at chloroplast membranes (Table 1; Figure 6c). H_2O_2 appears to mimic HL, in line with a report that H_2O_2 represents the major ROS species produced in HL-exposed *Chlamydomonas* cells (Chang et al., 2014). Hence, VIPP1/2 together with HSP22E/F may be involved in the prevention of oxidative damage and/or the clearing of oxidatively damaged membrane proteins and lipids. We can imagine three non-mutually exclusive modes of action by which this is accomplished (Figure 8):

i. The mere binding of proteins containing AHa domains, such as PspA and VIPP1, has been shown to alleviate SCE stress (Attard et al., 2000; Kirsten, Baron, Seabra, & Ces, 2013; McDonald et al., 2015). This is likely true also for VIPP1/2 oligomers binding to membranes in the chloroplast of HL- or H_2O_2-treated cells. With VIPP2 as a sensor and nucleation point, VIPP1 and HSP22E/F might populate areas suffering from SCE stress to prevent membrane leakage.

ii. With VIPP2 as a sensor for SCE stress caused by lipid/protein oxidation, VIPP1/2 together with HSP22E/F might protect membrane lipids/proteins from further oxidation by providing oxidizable methionines. HSP22E/F, VIPP1, and VIPP2 contain two, eight, and nine methionines, respectively (Figure S5). Oxidized methionines in VIPP1/2 and HSP22E/F might get re-reduced by the action of a peptide methionine sulfoxide reductase (PMSR). This scenario has been proposed previously for *Arabidopsis* Hsp21 under heat stress conditions, during which two-thirds of the otherwise stromal proteins re-localize to thylakoid membranes (Bernfur, Rutsdottir, & Emanuelsson, 2017). Hsp21 has an N-terminal amphipathic α-helix harbouring six methionines that can get oxidized by H_2O_2 and re-reduced by a plastid PMSR (Gustavsson et al., 2002; Harndahl et al., 1999), suggesting an Hsp21 methionine sulfoxidation-reduction cycle to quench reactive oxygen species (Sundby, Harndahl, Gustavsson, Ahrman, & Murphy, 2005). A similar mechanism has also been proposed for the membrane-localized Hsp16.3 in *Mycobacterium tuberculosis* (Abulimiti, Qiu, Chen, Liu, & Chang, 2003).

iii. We have shown previously that HSP22E/F binds thermolabile soluble chloroplast proteins as well as chaperones HSP70B and
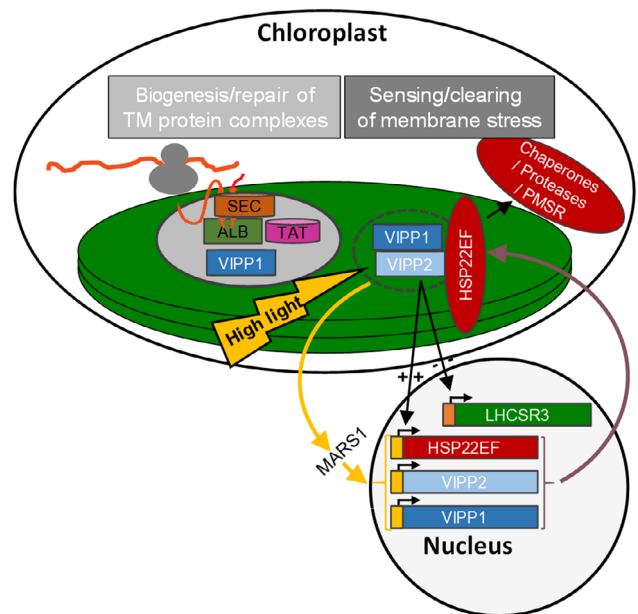

FIGURE 8 Hypothetical model for the role of VIPPs in *Chlamydomonas* chloroplasts. Chloroplast membranes are shown as green discs. We speculate on the existence of lipid domains organized largely by VIPP1 under normal growth conditions (grey disc) that attract translocases and integrases to support the biogenesis and repair of thylakoid membrane protein complexes. Under membrane stress conditions inflicted, for example, by high light intensities (dashed region), VIPP2 assembles heterooligomers with VIPP1 that form a complex with HSP22E/F to (i) alleviate membrane SCE stress; (ii) to protect membrane proteins/lipids from oxidative damage by providing oxidizable methionines that get re-reduced by a stromal peptide methionine sulfoxide reductase (PMSR); and (iii) to handle accumulating misfolded or unassembled proteins by providing an interface for the access of stromal chaperones and proteases. VIPP2 also signals the membrane stress state to the nucleus to modulate the expression of the *HSP22E/F* and *LHCSR3* genes. A retrograde signal triggered by high light is relayed by the MARS1 kinase (Perlaza et al., 2019)

CPN60B, most likely to prevent the formation of larger aggregates and to provide access for chaperones and proteases in order to refold and degrade aggregated proteins (Rütgers et al., 2017). Under conditions of oxidative stress, small HSPs have been shown to bind soluble enzymes and protect them from oxidative damage (Kitagawa, Miyakawa, Matsumura, & Tsuchido, 2002; Preville et al., 1999). At chloroplast membranes of HL- or H_2O_2-exposed cells, VIPP1/2 might organize membrane domains that serve as interfaces between membrane and soluble chaperones and proteases for the handling of oxidized, unfolded membrane proteins. DEG1C might be such a protease, as it accumulates under the same stress conditions as VIPP2 and localizes one third of its pool to chloroplast membranes (Figure 5b; Theis, Lang, et al., 2019). In fact, *Arabidopsis* Hsp21 has been shown to maintain the integrity of thylakoid membranes in the *gun5* mutant during heat stress, apparently by stabilizing PSII through direct interaction (Chen, He, Chen, & Guo, 2017). An

attractive aspect of scenarios (i) and (iii) is that they would also account for a role of VIPP1/2 and HSP22E/F under conditions not related to oxidative stress, for example, when unassembled subunits accumulate in *alb3* and *secA* mutants.

ORCID

Felix Willmund https://orcid.org/0000-0002-3988-4590
Benjamin D. Engel https://orcid.org/0000-0002-0941-4387
Michael Schroda https://orcid.org/0000-0001-6872-0483

REFERENCES

Abulimiti, A., Qiu, X., Chen, J., Liu, Y., & Chang, Z. (2003). Reversible methionine sulfoxidation of *Mycobacterium tuberculosis* small heat shock protein Hsp16.3 and its possible role in scavenging oxidants. *Biochemical and Biophysical Research Communications*, 305, 87–93.

Allorent, G., & Petroutsos, D. (2017). Photoreceptor-dependent regulation of photoprotection. *Current Opinion in Plant Biology*, 37, 102–108.

Asamizu, E., Miura, K., Kucho, K., Inoue, Y., Fukuzawa, H., Ohyama, K., ... Tabata, S. (2000). Generation of expressed sequence tags from low-CO₂ and high-CO₂ adapted cells of *Chlamydomonas reinhardtii*. *DNA Research*, 7, 305–307.

Aseeva, E., Ossenbuhl, F., Eichacker, L. A., Wanner, G., Soll, J., & Vothknecht, U. C. (2004). Complex formation of Vipp1 depends on its alpha-helical PspA-like domain. *Journal of Biological Chemistry*, 279, 35535–35541.

Aseeva, E., Ossenbuhl, F., Sippel, C., Cho, W. K., Stein, B., Eichacker, L. A., ... Vothknecht, U. C. (2007). Vipp1 is required for basic thylakoid membrane formation but not for the assembly of thylakoid protein complexes. *Plant Physiology and Biochemistry*, 45, 119–128.

Attard, G. S., Templer, R. H., Smith, W. S., Hunt, A. N., & Jackowski, S. (2000). Modulation of CTP:phosphocholine cytidylyltransferase by membrane curvature elastic stress. *Proceedings of the National Academy of Sciences of the United States of America*, 97, 9032–9036.

Bellafiore, S., Ferris, P., Naver, H., Gohre, V., & Rochaix, J. D. (2002). Loss of Albino3 leads to the specific depletion of the light-harvesting system. *Plant Cell*, 14, 2303–2314.

Bernfur, K., Rutsdottir, G., & Emanuelsson, C. (2017). The chloroplast-localized small heat shock protein Hsp21 associates with the thylakoid membranes in heat-stressed plants. *Protein Science*, 26, 1773–1784.

Bryan, S. J., Burroughs, N. J., Shevela, D., Yu, J., Rupprecht, E., Liu, L. N., ... Mullineaux, C. W. (2014). Localisation and interactions of the Vipp1 protein in cyanobacteria. *Molecular Microbiology*., 94, 1179–1195.

Chang, H. L., Tseng, Y. L., Ho, K. L., Shie, S. C., Wu, P. S., Hsu, Y. T., & Lee, T. M. (2014). Reactive oxygen species modulate the differential expression of methionine sulfoxide reductase genes in *Chlamydomonas reinhardtii* under high light illumination. *Physiologia Plantarum*, 150, 550–564.

Chen, S. T., He, N. Y., Chen, J. H., & Guo, F. Q. (2017). Identification of core subunits of photosystem II as action sites of HSP21, which is activated by the GUN5-mediated retrograde pathway in *Arabidopsis*. *Plant Journal*, 89, 1106–1118.

Cox, J., Hein, M. Y., Luber, C. A., Paron, I., Nagaraj, N., & Mann, M. (2014). MaxLFQ allows accurate proteome-wide label-free quantification by delayed normalization and maximal peptide ratio extraction. *Molecular & Cellular Proteomics*., 13, 2513–2526.

Cox, J., & Mann, M. (2008). MaxQuant enables high peptide identification rates, individualized p.p.b.-range mass accuracies and proteome-wide protein quantification. *Nature Biotechnology*, 26, 1367–1372.

Crozet, P., Navarro, F. J., Willmund, F., Mehrshahi, P., Bakowski, K., Lauersen, K. J., ... Lemaire, S. D. (2018). Birth of a photosynthetic chassis: A MoClo toolkit enabling synthetic biology in the microalga *Chlamydomonas reinhardtii*. *ACS Synthetic Biology*, 7, 2074–2086.

DeLisa, M. P., Lee, P., Palmer, T., & Georgiou, G. (2004). Phage shock protein PspA of *Escherichia coli* relieves saturation of protein export via the Tat pathway. *Journal of Bacteriology*, 186, 366–373.

Engl, C., Jovanovic, G., Lloyd, L. J., Murray, H., Spitaler, M., Ying, L., ... Buck, M. (2009). In vivo localizations of membrane stress controllers PspA and PspG in *Escherichia coli*. *Molecular Microbiology*, 73, 382–396.

Felsenstein, J. (1985). Confidence limits on phylogenies: An approach using the bootstrap. *Evolution*, 39, 783–791.

Fuhrmann, E., Bultema, J. B., Kahmann, U., Rupprecht, E., Boekema, E. J., & Schneider, D. (2009). The vesicle-inducing protein 1 from *Synechocystis sp.* PCC 6803 organizes into diverse higher-ordered ring structures. *Molecular Biology of the Cell*, 20, 4620–4628.

Fuhrmann, E., Gathmann, S., Rupprecht, E., Golecki, J., & Schneider, D. (2009). Thylakoid membrane reduction affects the photosystem stoichiometry in the cyanobacterium *Synechocystis sp.* PCC 6803. *Plant Physiology*, 149, 735–744.

Gao, F., Wang, W., Zhang, W., & Liu, C. (2015). Alpha-helical domains affecting the oligomerization of Vipp1 and its interaction with Hsp70/DnaK in *Chlamydomonas*. *Biochemistry*, 54, 4877–4889.

Gao, H., & Xu, X. (2009). Depletion of Vipp1 in *Synechocystis sp.* PCC 6803 affects photosynthetic activity before the loss of thylakoid membranes. *FEMS Microbiology Letters*, 292, 63–70.

Gautier, R., Douguet, D., Antonny, B., & Drin, G. (2008). HELIQUEST: A web server to screen sequences with specific α-helical properties. *Bioinformatics*, 24, 2101–2102.

Göhre, V., Ossenbuhl, F., Crevecoeur, M., Eichacker, L. A., & Rochaix, J. D. (2006). One of two alb3 proteins is essential for the assembly of the photosystems and for cell survival in *Chlamydomonas*. *Plant Cell*, 18, 1454–1466.

Gustavsson, N., Kokke, B. P., Harndahl, U., Silow, M., Bechtold, U., Poghosyan, Z., ... Sundby, C. (2002). A peptide methionine sulfoxide reductase highly expressed in photosynthetic tissue in *Arabidopsis thaliana* can protect the chaperone-like activity of a chloroplast-localized small heat shock protein. *Plant Journal*, 29, 545–553.

Gutu, A., Chang, F., & O'Shea, E. K. (2018). Dynamical localization of a thylakoid membrane binding protein is required for acquisition of photosynthetic competency. *Molecular Microbiology*., 108, 16–31.

Hankamer, B. D., Elderkin, S. L., Buck, M., & Nield, J. (2004). Organization of the AAA(+) adaptor protein PspA is an oligomeric ring. *Journal of Biological Chemistry*, 279, 8862–8866.

Harndahl, U., Hall, R. B., Osteryoung, K. W., Vierling, E., Bornman, J. F., & Sundby, C. (1999). The chloroplast small heat shock protein undergoes oxidation-dependent conformational changes and may protect plants from oxidative stress. *Cell Stress and Chaperones*, 4, 129–138.

Hemme, D., Veyel, D., Mühlhaus, T., Sommer, F., Juppner, J., Unger, A. K., ... Schroda, M. (2014). Systems-wide analysis of acclimation responses to long-term heat stress and recovery in the photosynthetic model organism *Chlamydomonas reinhardtii*. *Plant Cell*, 26, 4270–4297.

Hennig, R., Heidrich, J., Saur, M., Schmuser, L., Roeters, S. J., Hellmann, N., ... Schneider, D. (2015). IM30 triggers membrane fusion in cyanobacteria and chloroplasts. *Nature Communications*, 6, 7018.

Jovanovic, G., Mehta, P., McDonald, C., Davidson, A. C., Uzdavinys, P., Ying, L., & Buck, M. (2014). The N-terminal amphipathic helices determine regulatory and effector functions of phage shock protein A (PspA) in *Escherichia coli*. *Journal of Molecular Biology*, 426, 1498–1511.

Kindle, K. L. (1990). High-frequency nuclear transformation of *Chlamydomonas reinhardtii*. *Proceedings of the National Academy of Sciences of the United States of America*, 87, 1228–1232.

Kirsten, M. L., Baron, R. A., Seabra, M. C., & Ces, O. (2013). Rab1a and Rab5a preferentially bind to binary lipid compositions with higher stored curvature elastic energy. *Molecular Membrane Biology*, 30, 303–314.

Kitagawa, M., Miyakawa, M., Matsumura, Y., & Tsuchido, T. (2002). *Escherichia coli* small heat shock proteins, IbpA and IbpB, protect enzymes from inactivation by heat and oxidants. *European Journal of Biochemistry*, 269, 2907–2917.

Kleerebezem, M., Crielaard, W., & Tommassen, J. (1996). Involvement of stress protein PspA (phage shock protein A) of *Escherichia coli* in maintenance of the protonmotive force under stress conditions. *EMBO Journal*, 15, 162–171.

Kobayashi, R., Suzuki, T., & Yoshida, M. (2007). *Escherichia coli* phage-shock protein A (PspA) binds to membrane phospholipids and repairs proton leakage of the damaged membranes. *Molecular Microbiology*, 66, 100–109.

Kroll, D., Meierhoff, K., Bechtold, N., Kinoshita, M., Westphal, S., Vothknecht, U. C., ... Westhoff, P. (2001). VIPP1, a nuclear gene of *Arabidopsis thaliana* essential for thylakoid membrane formation. *Proceedings of the National Academy of Sciences of the United States of America*, 98, 4238–4242.

Kropat, J., Hong-Hermesdorf, A., Casero, D., Ent, P., Castruita, M., Pellegrini, M., ... Malasarn, D. (2011). A revised mineral nutrient supplement increases biomass and growth rate in *Chlamydomonas reinhardtii*. *Plant Journal*, 66, 770–780.

Kumar, S., Stecher, G., & Tamura, K. (2016). MEGA7: Molecular Evolutionary Genetics Analysis Version 7.0 for bigger datasets. *Molecular Biology and Evolution*, 33, 1870–1874.

Laemmli, U. K. (1970). Cleavage of structural proteins during the assembly of the head of bacteriophage T4. *Nature*, 227, 680–685.

Lemaire, C., & Wollman, F. A. (1989). The chloroplast ATP synthase in *Chlamydomonas reinhardtii*. I. Characterization of its nine constitutive subunits. *Journal of Biological Chemistry*, 264, 10228–10234.

Li, H. M., Kaneko, Y., & Keegstra, K. (1994). Molecular cloning of a chloroplastic protein associated with both the envelope and thylakoid membranes. *Plant Molecular Biology*, 25, 619–632.

Li, X., Zhang, R., Patena, W., Gang, S. S., Blum, S. R., Ivanova, N., ... Jonikas, M. C. (2016). An indexed, mapped mutant library enables reverse genetics studies of biological processes in *Chlamydomonas reinhardtii*. *Plant Cell*, 28, 367–387.

Liu, C., Willmund, F., Golecki, J. R., Cacace, S., Hess, B., Markert, C., & Schroda, M. (2007). The chloroplast HSP70B-CDJ2-CGE1 chaperones catalyse assembly and disassembly of VIPP1 oligomers in *Chlamydomonas*. *Plant Journal*, 50, 265–277.

Liu, C., Willmund, F., Whitelegge, J. P., Hawat, S., Knapp, B., Lodha, M., & Schroda, M. (2005). J-domain protein CDJ2 and HSP70B are a plastidic chaperone pair that interacts with vesicle-inducing protein in plastids 1. *Molecular Biology of the Cell*, 16, 1165–1177.

Lo, S. M., & Theg, S. M. (2012). Role of vesicle-inducing protein in plastids 1 in cpTat transport at the thylakoid. *Plant Journal*, 71, 656–668.

Lowry, O. H., Rosebrough, N. J., Farr, A. L., & Randall, R. J. (1951). Protein measurement with the Folin phenol reagent. *Journal of Biological Chemistry*, 193, 265–275.

Male, A. L., Oyston, P. C. F., & Tavassoli, A. (2014). Self-assembly of *Escherichia coli* Phage Shock Protein A. *Advances in Microbiology*, 04, 353–359.

Manganelli, R., & Gennaro, M. L. (2017). Protecting from envelope stress: Variations on the Phage-Shock-Protein Theme. *Trends in Microbiology*, 25, 205–216.

Maruyama, S., Tokutsu, R., & Minagawa, J. (2014). Transcriptional regulation of the stress-responsive light harvesting complex genes in *Chlamydomonas reinhardtii*. *Plant and Cell Physiology*, 55, 1304–1310.

McDonald, C., Jovanovic, G., Ces, O., & Buck, M. (2015). Membrane stored curvature elastic stress modulates recruitment of maintenance proteins PspA and Vipp1. *MBio*, 6, e01188–e01115.

McDonald, C., Jovanovic, G., Wallace, B. A., Ces, O., & Buck, M. (2017). Structure and function of PspA and Vipp1 N-terminal peptides: Insights into the membrane stress sensing and mitigation. *Biochimica et Biophysica Acta*, 1859, 28–39.

Müller, N., Leroch, M., Schumacher, J., Zimmer, D., Konnel, A., Klug, K., ... Hahn, M. (2018). Investigations on VELVET regulatory mutants confirm the role of host tissue acidification and secretion of proteins in the pathogenesis of *Botrytis cinerea*. *The New Phytologist*, 219, 1062–1074.

Muranaka, L. S., Rutgers, M., Bujaldon, S., Heublein, A., Geimer, S., Wollman, F. A., & Schroda, M. (2016). TEF30 interacts with photosystem II monomers and is involved in the repair of photodamaged photosystem II in *Chlamydomonas reinhardtii*. *Plant Physiology*, 170, 821–840.

Naumann, B., Busch, A., Allmer, J., Ostendorf, E., Zeller, M., Kirchhoff, H., & Hippler, M. (2007). Comparative quantitative proteomics to investigate the remodeling of bioenergetic pathways under iron deficiency in *Chlamydomonas reinhardtii*. *Proteomics*, 7, 3964–3979.

Nordhues, A., Schöttler, M. A., Unger, A. K., Geimer, S., Schönfelder, S., Schmollinger, S., ... Schroda, M. (2012). Evidence for a role of VIPP1 in the structural organization of the photosynthetic apparatus in *Chlamydomonas*. *Plant Cell*, 24, 637–659.

Ossenbühl, F., Gohre, V., Meurer, J., Krieger-Liszkay, A., Rochaix, J. D., & Eichacker, L. A. (2004). Efficient assembly of photosystem II in *Chlamydomonas reinhardtii* requires Alb3.1p, a homolog of *Arabidopsis* ALBINO3. *Plant Cell*, 16, 1790–1800.

Otters, S., Braun, P., Hubner, J., Wanner, G., Vothknecht, U. C., & Chigri, F. (2013). The first alpha-helical domain of the vesicle-inducing protein in plastids 1 promotes oligomerization and lipid binding. *Planta*, 237, 529–540.

Peers, G., Truong, T. B., Ostendorf, E., Busch, A., Elrad, D., Grossman, A. R., ... Niyogi, K. K. (2009). An ancient light-harvesting protein is critical for the regulation of algal photosynthesis. *Nature*, 462, 518–521.

Perlaza K., Toutkoushian H., Boone M., Lam M., Iwai M., Jonikas M.C., Walter P. & Ramundo S. (2019) The Mars1 kinase confers photoprotection through signaling in the chloroplast unfolded protein response. *Elife*, 8.

Pierre, Y., & Popot, J. L. (1993). Identification of two 4-kDa miniproteins in the cytochrome b_6f complex from *Chlamydomonas reinhardtii*. *Comptes Rendus de l'Académie Des Sciences. Série III: Sciences de la Vie*, 316, 1404–1409.

Preville, X., Salvemini, F., Giraud, S., Chaufour, S., Paul, C., Stepien, G., ... Arrigo, A. P. (1999). Mammalian small stress proteins protect against oxidative stress through their ability to increase glucose-6-phosphate dehydrogenase activity and by maintaining optimal cellular detoxifying machinery. *Experimental Cell Research*, 247, 61–78.

Ramundo, S., Casero, D., Mühlhaus, T., Hemme, D., Sommer, F., Crevecoeur, M., ... Rochaix, J. D. (2014). Conditional depletion of the *Chlamydomonas* chloroplast ClpP protease activates nuclear genes involved in autophagy and plastid protein quality control. *Plant Cell*, 26, 2201–2222.

Rütgers, M., Muranaka, L. S., Mühlhaus, T., Sommer, F., Thoms, S., Schurig, J., ... Schroda, M. (2017). Substrates of the chloroplast small heat shock proteins 22E/F point to thermolability as a regulative switch for heat acclimation in *Chlamydomonas reinhardtii*. *Plant Molecular Biology*, 95, 579–591.

Rütgers, M., & Schroda, M. (2013). A role of VIPP1 as a dynamic structure within thylakoid centers as sites of photosystem biogenesis? *Plant Signaling & Behavior*, 8, e27037.

Saitou, N., & Nei, M. (1987). The neighbor-joining method: A new method for reconstructing phylogenetic trees. *Molecular Biology and Evolution*, 4, 406–425.

Saur, M., Hennig, R., Young, P., Rusitzka, K., Hellmann, N., Heidrich, J., … Schneider, D. (2017). A Janus-faced IM30 ring involved in thylakoid membrane fusion is assembled from IM30 tetramers. *Structure*, *25* (1380–1390), e1385.

Schmollinger, S., Strenkert, D., & Schroda, M. (2010). An inducible artificial microRNA system for *Chlamydomonas reinhardtii* confirms a key role for heat shock factor 1 in regulating thermotolerance. *Current Genetics*, *56*, 383–389.

Schroda, M., Hemme, D., & Mühlhaus, T. (2015). The *Chlamydomonas* heat stress response. *Plant Journal*, *82*, 466–480.

Schroda, M., Vallon, O., Whitelegge, J. P., Beck, C. F., & Wollman, F. A. (2001). The chloroplastic GrpE homolog of *Chlamydomonas*: Two isoforms generated by differential splicing. *Plant Cell*, *13*, 2823–2839.

Schroda, M., Vallon, O., Wollman, F. A., & Beck, C. F. (1999). A chloroplast-targeted heat shock protein 70 (HSP70) contributes to the photoprotection and repair of photosystem II during and after photoinhibition. *Plant Cell*, *11*, 1165–1178.

Srivastava, R., Pisareva, T., & Norling, B. (2005). Proteomic studies of the thylakoid membrane of Synechocystis sp. PCC 6803. *Proteomics*, *5*, 4905–4916.

Strenkert, D., Schmollinger, S., Sommer, F., Schulz-Raffelt, M., & Schroda, M. (2011). Transcription factor dependent chromatin remodeling at heat shock and copper responsive promoters in *Chlamydomonas reinhardtii*. *Plant Cell*, *23*, 2285–2301.

Sundby, C., Harndahl, U., Gustavsson, N., Ahrman, E., & Murphy, D. J. (2005). Conserved methionines in chloroplasts. *Biochimica et Biophysica Acta*, *1703*, 191–202.

Theis, J., Gupta, T. K., Klingler, J., Wan, W., Albert, S., Keller, S., … Schroda, M. (2019). VIPP1 rods engulf membranes containing phosphatidylinositol phosphates. *Scientific Reports*, *9*, 8725.

Theis, J., Lang, J., Spaniol, B., Ferte, S., Niemeyer, J., Sommer, F., … Schroda, M. (2019). The *Chlamydomonas deg1c* mutant accumulates proteins involved in high light acclimation. *Plant Physiology*, *18m*, 1480–1497.

Theis, J., & Schroda, M. (2016). Revisiting the photosystem II repair cycle. *Plant Signaling & Behavior*, *11*, e1218587.

Uniacke, J., Colon-Ramos, D., & Zerges, W. (2011). FISH and immunofluorescence staining in Chlamydomonas. *Methods in Molecular Biology*, *714*, 15–29.

Vrancken, K., De Keersmaeker, S., Geukens, N., Lammertyn, E., Anne, J., & Van Mellaert, L. (2007). pspA overexpression in *Streptomyces lividans* improves both Sec- and Tat-dependent protein secretion. *Applied Microbiology and Biotechnology*, *73*, 1150–1157.

Walter, B., Hristou, A., Nowaczyk, M. M., & Schunemann, D. (2015). In vitro reconstitution of co-translational D1 insertion reveals a role of the cpSec-Alb3 translocase and Vipp1 in photosystem II biogenesis. *Biochemical Journal*, *468*, 315–324.

Waterhouse, A. M., Procter, J. B., Martin, D. M., Clamp, M., & Barton, G. J. (2009). Jalview Version 2—A multiple sequence alignment editor and analysis workbench. *Bioinformatics*, *25*, 1189–1191.

Weber, E., Engler, C., Gruetzner, R., Werner, S., & Marillonnet, S. (2011). A modular cloning system for standardized assembly of multigene constructs. *PLoS One*, *6*, e16765.

Westphal, S., Heins, L., Soll, J., & Vothknecht, U. C. (2001). Vipp1 deletion mutant of *Synechocystis*: A connection between bacterial phage shock and thylakoid biogenesis? *Proceedings of the National Academy of Sciences of the United States of America*, *98*, 4243–4248.

Willmund, F., & Schroda, M. (2005). HEAT SHOCK PROTEIN 90C is a bona fide Hsp90 that interacts with plastidic HSP70B in *Chlamydomonas reinhardtii*. *Plant Physiology*, *138*, 2310–2322.

Wong-Ekkabut, J., Xu, Z., Triampo, W., Tang, I. M., Tieleman, D. P., & Monticelli, L. (2007). Effect of lipid peroxidation on the properties of lipid bilayers: A molecular dynamics study. *Biophysical Journal*, *93*, 4225–4236.

Zhang, L., Kato, Y., Otters, S., Vothknecht, U. C., & Sakamoto, W. (2012). Essential role of VIPP1 in chloroplast envelope maintenance in *Arabidopsis*. *Plant Cell*, *24*, 3695–3707.

Zhang, L., Kondo, H., Kamikubo, H., Kataoka, M., & Sakamoto, W. (2016). VIPP1 has a disordered C-terminal tail necessary for protecting photosynthetic membranes against stress. *Plant Physiology*, *171*, 1983–1995.

Zhang, L., Kusaba, M., Tanaka, A., & Sakamoto, W. (2016). Protection of chloroplast membranes by VIPP1 rescues aberrant seedling development in *Arabidopsis* nyc1 mutant. *Frontiers in Plant Science*, *7*, 533.

Zhang, L., & Sakamoto, W. (2013). Possible function of VIPP1 in thylakoids: Protection but not formation? *Plant Signaling & Behavior*, *8*, e22860.

Zhang, S., Shen, G., Li, Z., Golbeck, J. H., & Bryant, D. A. (2014). Vipp1 is essential for the biogenesis of Photosystem I but not thylakoid membranes in *Synechococcus* sp. PCC 7002. *Journal of Biological Chemistry*, *289*, 15904–15914.

Zuckerkandl, E., & Pauling, L. (1965). Molecules as documents of evolutionary history. *Journal of Theoretical Biology*, *8*, 357–366.

SUPPORTING INFORMATION

Additional supporting information may be found online in the Supporting Information section at the end of this article.